Pontifícia Universidade Católica
do Rio de Janeiro

David Fernando Porlles López

Optical detection of quantum geometrical properties in singlet superconductors

Dissertação de Mestrado

Dissertation presented to the Programa de Pós–graduação em Física of PUC-Rio in partial fulfillment of the requirements for the degree of Mestre em Ciências - Física.

Advisor: Prof. Wei Chen

Rio de Janeiro
March 2024

Pontifícia Universidade Católica
do Rio de Janeiro

David Fernando Porlles López

Optical detection of quantum geometrical properties in singlet superconductors

Dissertation presented to the Programa de Pós–graduação em Física of PUC-Rio in partial fulfillment of the requirements for the degree of Mestre em Ciências - Física. Approved by the Examination Committee:

Prof. Wei Chen
Advisor
Departamento de Física – PUC-Rio

Prof. Mucio Amado Continentino
CBPF

Prof. Evandro Vidor Lins de Mello
UFF

Rio de Janeiro, March 15th, 2024

David Fernando Porlles López

The author graduated in Physics from the Universidad Nacional Mayor de San Marcos (Lima, Peru) in 2019.

Bibliographic data

Porlles López, David Fernando

Optical detection of quantum geometrical properties in singlet superconductors / David Fernando Porlles López; advisor: Wei Chen. – 2024.

60 f: il. color. ; 30 cm

Dissertação (mestrado) - Pontifícia Universidade Católica do Rio de Janeiro, Departamento de Física, 2024.

Inclui bibliografia

1. Física – Teses. 2. Supercondutores. 3. Absorção infravermelha. 4. Geometria quântica. 5. Corrente paramagnética. 6. Função dielétrica. 7. Supercondutividade de alta temperatura. I. Chen, Wei. II. Pontifícia Universidade Católica do Rio de Janeiro. Departamento de Física. III. Título.

CDD: 530

Acknowledgments

I would like to express my sincerest gratitude to all those who have made the realization of this work possible. First and foremost, my infinite gratitude goes to my parents, who have been my source of inspiration and constant motivation. Their unconditional love, sacrifice, and belief in my capabilities have provided me with the strength to face challenges and move forward. Thank you for always being there, for your tireless support, and for teaching me the value of perseverance and dedication.

To my siblings, I extend my deepest thanks. Your support, understanding, and advice have been essential in my life and have greatly assisted me academically. To my brother Daniel, for your teachings and wisdom that have been a constant source of inspiration, helping me to overcome obstacles and keep my eyes on my goals.

I must also deeply acknowledge and thank my advisor, whose expert guidance and patience have been crucial in the development of this work. His willingness to share his time, knowledge, and experience has greatly enriched my learning and has been decisive in my professional growth. I sincerely appreciate his guidance, support, and confidence placed in me throughout this process.

This study was financed in part by the Coordenação de Aperfeiçoamento de Pessoal de Nível Superior - Brasil (CAPES) - Finance Code 001, and by the Fundação de Amparo à Pesquisa do Estado do Rio de Janeiro (FAPERJ).

Abstract

Porlles López, David Fernando; Chen, Wei (Advisor). **Optical detection of quantum geometrical properties in singlet superconductors**. Rio de Janeiro, 2024. 60p. Dissertação de Mestrado – Departamento de Física, Pontifícia Universidade Católica do Rio de Janeiro.

Quantum geometry in condensed matter physics allows us to understand various geometric properties of the Brillouin zone states, such as the Berry curvature and the quantum metric. Especially in relation to the latter, studies have been observed that show its relationship with superconductivity. Motivated by these investigations, this dissertation aims to investigate the quantum geometric properties of singlet superconductors, such as s-wave and d-wave types, and identify their relation to various electromagnetic responses. We begin by showing the description of these superconductors through mean field theory, subsequently analyzing their quantum metric, which is defined by the overlap of two quasihole states at slightly different momenta. Subsequently, we study the fidelity number, which is defined as the momentum integration of the quantum metric and represents the average distance between neighboring quasihole states. Furthermore, we express this fidelity number as a fidelity marker defined locally at each lattice site, which allows us to observe the effect of non-magnetic impurities on this marker. For s-wave superconductors, we show that electromagnetic responses such as infrared absorption are related to the quantum metric, while on the other hand, the paramagnetic current and the dielectric function are related to the fidelity number, which in turn is determined by the coherence length. On the other hand, for d-wave superconductors, we observe that their quantum metric shows a singular behavior and that their fidelity number diverges. The most relevant result of this dissertation is that we have discovered that singlet superconductors, described by the BCS mean field theory, exhibit a nontrivial quantum metric, and that for s-wave superconductors the aforementioned electromagnetic responses are directly related to the quantum geometry, which has not been found previously.

Keywords

Superconductors; Infrared absorption; Quantum geometry; Paramagnetic current; Dielectric function; High temperature superconductivit.

Resumo

Porlles López, David Fernando; Chen, Wei. **Detecção óptica de propriedades geométricas quânticas em supercondutores singletos**. Rio de Janeiro, 2024. 60p. Dissertação de Mestrado – Departamento de Física, Pontifícia Universidade Católica do Rio de Janeiro.

A geometria quântica na física da matéria condensada nos permite entender várias propriedades geométricas dos estados da zona de Brillouin, como a curvatura de Berry e a métrica quântica. Especialmente em relação a esta última, foram observados estudos que mostram sua relação com a supercondutividade. Motivados por estas investigações, esta dissertação visa investigar as propriedades geométricas quânticas de supercondutores singletos, como os tipos s-wave e d-wave, e identificar sua relação com várias respostas eletromagnéticas. Começamos mostrando a descrição desses supercondutores através da teoria do campo médio, posteriormente analisando sua métrica quântica, que é definida pela sobreposição de dois estados de *quasihole* em momentos ligeiramente diferentes. Subsequentemente, estudamos o número de fidelidade, que é definido como a integração de momento da métrica quântica e representa a distância média entre estados de *quasihole* vizinhos. Além disso, expressamos esse número de fidelidade como um marcador de fidelidade definido localmente em cada sítio da rede, o que nos permite observar o efeito de impurezas não magnéticas nesse marcador. Para supercondutores de tipo s-wave, mostramos que respostas eletromagnéticas como a absorção no infravermelho estão relacionadas à métrica quântica, enquanto, por outro lado, a corrente paramagnética e a função dielétrica estão relacionadas ao número de fidelidade, que por sua vez é determinado pelo comprimento de coerência. Por outro lado, para supercondutores de tipo d-wave, observamos que sua métrica quântica mostra um comportamento singular e que seu número de fidelidade diverge. O resultado mais relevante desta dissertação é que descobrimos que supercondutores singletos, descritos pela teoria do campo médio BCS, exibem uma métrica quântica não trivial, e que para supercondutores de tipo s-wave as respostas eletromagnéticas mencionadas estão diretamente relacionadas à geometria quântica, o que não havia sido encontrado anteriormente.

Palavras-chave

Supercondutores; Absorção infravermelha; Geometria quântica; Corrente paramagnética; Função dielétrica; Supercondutividade de alta temperatura.

Table of contents

List of figures

1
Introduction

Quantum geometry holds significant relevance in condensed matter physics, providing an understanding of various properties such as Berry phases, quantum metric, among others. For the study of quantum geometry, we utilize the quantum geometric tensor, the first notions of which were introduced in 1980 [1]. For this, we consider a Hamiltonian described by some parameter λ, then the measure of the distance between two neighboring states $|\psi(\lambda)\rangle$ and $|\psi(\lambda+\delta\lambda)\rangle$ is given by

$$ds^2 = 1 - |\langle\psi(\lambda)||\psi(\lambda+\delta\lambda)\rangle|^2 = \sum_{\mu\nu} T_{\mu\nu} d\lambda^\mu d\lambda^\nu, \tag{1-1}$$

where $T_{\mu\nu}$ is the quantum geometric tensor, which can be expressed as $T_{\mu\nu} = g_{\mu\nu} - \frac{i}{2}F_{\mu\nu}$ [2, 3, 4]. The imaginary part of $T_{\mu\nu}$ is antisymmetric and is related to the Berry curvature $F_{\mu\nu} = 2\mathrm{Im}T_{\mu\nu}$, which is responsible for phenomena such as Hall effects [5, 6], and related to electronic properties [5] and topological phases of matter [7, 8]. On the other hand, the real part of this term is symmetric and corresponds to the quantum metric $g_{\mu\nu} = \mathrm{Re}[T_{\mu\nu}]$, which also arises equivalently from the following expression $|\langle\psi(\lambda)|\psi(\lambda+\delta\lambda)\rangle| = 1 - \frac{1}{2}g_{\mu\nu}\delta\lambda^\mu d\lambda^\nu$, for solids, we use momentum space hamiltonian and Bloch eigenstate to define this quantum metric.

This quantum metric can also be related to various experimental measures [9, 10, 11, 12]. For example, there are investigations that show how to relate the metric to optical responses by introducing a term called the quantum metric spectral function $g^d_{\mu\nu}(k,\omega)$ [13, 14, 15], where the superscript d is because the system is considered to be "dressed" by interactions. For the case of a gap material, referred to as those materials that exhibit a gap in their electronic structure, it is possible to relate the quantum metric spectral function, that frequency-integrates to the quantum metric, with the exciton absorption rate [13]. Also, the momentum integration of the quantum metric spectral function gives us a term called the fidelity number spectral function $G^d_{\mu\nu}(\omega)$, which is related to the frequency dependence of the optical absorption rate [14].

Another closely related term is the fidelity number, which is defined as the momentum integral of the quantum metric over a toroid T^D. This toroid

represents the D-dimensional Brillouin zone manifold, which physically represents the average distance between neighboring Bloch states in momentum space. We can express this quantity in real space through the projection formalism to define a fidelity marker at each lattice site, which allows us to study, for example, the influence of impurities in real space on the quantum geometrical properties [15].

On the other hand, it has also been found that the quantum metric is related to topological order. This is a type of order that represents a certain geometric property of the Bloch state in momentum space [16], and depending on the dimension and symmetry of the system [17, 18, 19, 20]. This order can manifest through different physical phenomena. In systems characterized by a topological order derived from the integration of the Berry connection or Berry curvature in momentum space, the determinant of the quantum metric is related to these quantities [21, 22, 23, 24]. In relation to the aforementioned, it has been found that in Dirac models, when the integration of a certain function with respect to momentum result in a topological order, the modulus of that function is equal to the determinant of the quantum metric. This relationship has been called the metric-curvature correspondence [16]. Thus, as mentioned earlier, the spectral quantum metric function that allows us to measure the exciton absorption can also serve to reveal the topological order through this correspondence.

Recent research in the field of superconductivity has begun to employ concepts of quantum geometry to explain and predict behaviors in superconductors [25, 26, 27]. Before delving into these investigations, it is pertinent to briefly discuss on superconductors.

Superconductors are classified into conventional and unconventional types. On one hand, we have the conventional superconductors, which are studied using the BCS theory and, due to the isotropic nature of the Cooper pairs wave function, are known as s-wave superconductors. On the other hand, we have the unconventional superconductors, which encompass all other types of superconductors, such as those of the d-wave and p-wave types. However, for a large number of materials, they can still be described by a weak coupling mean field theory similar to the BCS theory.

Moreover, in recent years, it has been discovered the relationship between the metric and flat band superconductors. This type of material exhibits a flat band in its normal state, which is relevant because this type of superconductivity has been recently found in twisted bilayer graphene [28, 29]. The explanation of how superconductivity arises in these materials is still under study; however, there have been several investigations showing that the superfluid

density in a flat band is proportional to the quantum metric [30, 31, 32].

Motivated by the aforementioned investigations on the relationship between the quantum metric with the exciton absorption rate in gap materials, as well as the research on flat band superconductors regarding the relationship between the superfluid density and the quantum metric, this dissertation delves into the quantum geometric properties of the quasihole band in singlet superconductors. It aims to study the quantum geometric properties of singlet superconductors such as s-wave and d-wave superconductors, as well as to observe if these properties are related to different electromagnetic responses.

As a significant outcome of our work, we have discovered that singlet superconductors, described by the mean field BCS theory, exhibit a nontrivial quantum metric, which furthermore is ubiquitously present in the electromagnetic responses of s-wave superconductors. This constitutes a novel finding that has not been previously identified. Additionally, a significant finding derived from the study of s-wave type superconductors is the observation that the fidelity number can be expressed as a function of the coherence length. This allows us to establish an important conclusion in which the properties linked to the coherence length also have a direct relationship with the fidelity number.

This dissertation is organized as follows. In Chapter 2, we review superconductivity, covering London's theory, BCS theory, and singlet superconductors. In Chapter 3, we study the quantum geometric properties of singlet superconductors such as the quantum metric, the fidelity number, and the fidelity marker. We will also see how these quantities behave in the case of an s-wave and d-wave superconductor. In Chapter 4, we show how some electromagnetic responses, such as infrared absorption, paramagnetic current, and the dielectric function, are related to some of the quantum geometric quantities seen in Chapter 3. In Chapter 5 we present the final conclusions as well as the perspectives for future works.

Additionally, the dissertation is complemented with three appendices. In appendix A, we show the form of the polarization operator for singlet superconductors. In appendix B, we briefly explain the conductivity and the dielectric function of a non-interacting electron gas. Finally, in appendix C, we demonstrate how to obtain analytical expressions for some quantities of both quantum geometry and electromagnetic responses for s-wave superconductors. These appendices provide complementary information and several findings will be used throughout the dissertation.

2
Superconductivity

In this chapter, we will conduct a review of superconductivity. Subsequently, we will discuss the BCS theory in more detail, showing the superconducting gap equation obtained through the Bogoliubov transformation. In the final section, we will talk about singlet superconductors, such as those of s-wave and d-wave types.

2.1
Brief introduction of Superconductivity

In 1908, Dutch physicist Heike Kamerlingh Onnes succeeded in liquefying helium at a temperature of 4.1 K, thus enabling the study of the properties of various metals at very low temperatures [33]. A few years later, in 1911, Kamerlingh Onnes observed that the electrical resistance of Hg abruptly fell to zero at a critical temperature of approximately 4.18 K [34]. This phase of matter was subsequently named the superconducting state and was found in other materials such as Sn, Pb, Tl [35].

In 1933, the Meissner effect was discovered by Walter Meissner and Robbert Ochsenfeld [36]. This effect was observed experimentally and establishes that superconductors behave as perfect diamagnets. This means that when a material is in its superconducting phase and a magnetic field is applied, this field is expelled from the material. Depending on whether the expulsion of the field is total or partial, they can be classified as type I and II superconductors.

There were several attempts to explain the phenomenon of superconductivity. In 1935, the brothers Fritz and Heinz London developed the first phenomenological theory of superconductivity [37]. This theory explains the Meissner effect and predicts how far an external magnetic field can penetrate a superconductor. Years later, in 1950, Vitaly Ginzburg and Lev Landau proposed a phenomenological theory that expanded Landau's phase transition theory, applying it to superconductivity [38, 39]. This theory introduces an order parameter that varies in space, with its variations and properties described by a specific equation. This equation is fundamental in explaining the Meissner effect, where superconductors expel magnetic fields upon cooling below their critical temperature. Additionally, the Ginzburg-Landau theory is crucial for

calculating fundamental properties like the critical temperature and critical magnetic field, and it is notable for predicting the formation of superconducting vortices in Type II superconductors subjected to intense magnetic fields.

In 1950, due to several experimental works [40, 41], the isotopic effect was discovered, this effect predicted that the superconductor transition temperature would decrease with an increase in the average isotopic mass of the material. The inverse relationship between the transition temperature and the isotopic mass supports the idea that the electron-phonon interaction is essential in superconductivity. The isotopic effect serves as key evidence that phonons (quanta of lattice vibrations) are involved in the pairing of electrons that form the superconducting state.

Currently, our theoretical understanding of superconductivity is largely based on the microscopic BCS (Bardeen, Cooper, and Schrieffer) theory, formulated in 1957 [42]. The role of the electron-phonon interaction in the formation of these pairs is central in the BCS theory, thereby providing a coherent explanation for the observed isotopic effect.

In the following sections, we will first delve into London's theory, followed by an exploration of the BCS theory, starting from the concept of Cooper pairs and then advancing to calculations derived from this theory.

2.2 London's theory

As mentioned earlier, one of the first theories to explain the phenomenon of superconductivity was developed by the London brothers. This theory describes the electromagnetic behavior of a superconductor [36].

In this theory, the existence of two independent types of electrons is assumed: the so-called superconducting electrons, which move through the superconductor without dissipation, and the normal electrons, which are associated with energy dissipation in the form of electrical resistance.

The density of normal electrons will be denoted as n_n, and that of superconducting electrons as n_s. The normal current density obeys Ohm's law

$$\mathbf{J}_n = \sigma_n \mathbf{E}. \tag{2-1}$$

On the other hand, superconducting electrons when an electric field $\mathbf{E}$ is applied have the following equation of motion

$$m\frac{d\mathbf{v}_s}{dt} = -e\mathbf{E}, \tag{2-2}$$

where e is the charge of the electron, m is the mass of the electron, and v_s is the velocity of the electron in the superconducting state. Furthermore, the

current density is defined as

$$\mathbf{J}_s = -en_s\mathbf{v}_s, \tag{2-3}$$

differentiating it with respect to time and using the equation of motion we have

$$\frac{d\mathbf{J}_s}{dt} = \frac{n_s e^2}{m}\mathbf{E}, \tag{2-4}$$

this is the first London equation and indicates that in the presence of an electric field a superconducting current is induced that varies over time and that the current flows without resistance.

Now we calculate the time derivative of $\nabla \times \mathbf{J}_s$ and considering Faraday's law of magnetic induction $\nabla \times \mathbf{E} = -\partial\mathbf{B}/\partial t$, we obtain

$$\frac{d(\nabla \times \mathbf{J}_s)}{dt} = -\frac{n_s e^2}{m}\frac{\partial \mathbf{B}}{\partial t}, \tag{2-5}$$

we proceed to integrate with respect to time, the London brothers to arrive at the results of the Meissner effect postulated that the integration constant should be zero obtaining

$$\nabla \times \mathbf{J}_s = -\frac{n_s e^2}{m}\mathbf{B}, \tag{2-6}$$

this equation is the second London equation and describes how an applied magnetic field induces a superconducting current on the surface of the material, which in turn generates an opposing magnetic field that cancels the applied magnetic field inside the superconductor explaining the Meissner effect.

2.3 BCS theory

In 1957, the BCS theory, named after its discoverers Bardeen, Cooper, and Schrieffer, was formulated as the first theory to explain superconductivity from a microscopic viewpoint [42]. This theory accurately predicts various properties of superconductors. Furthermore, it serves as the foundation from which the Ginzburg-Landau theory can be derived. Subsequently, we will delve deeper into this theory.

The BCS theory is based on two bound electrons called Cooper pairs. In the following section, I will address more about Cooper pairs. These pairs form a collective quantum state that extends throughout the material. The coherence of this collective quantum state is crucial, as it prevents the scattering of electrons that would cause resistance in normal conductors.

Moreover, an energy gap forms at the Fermi level, known as the "superconducting gap". This gap represents an energy difference between the highest state of the Cooper pairs and the lowest electronic state above the gap. In other words, there is an energy region where no electronic states are available.

The existence of this gap is crucial because it impedes certain types of electron scattering that would cause resistance in a normal conductor.

2.3.1 Cooper Pairs

The concept of Cooper pairs, proposed by physicist Leon Cooper in 1956, represents a cornerstone in the understanding of superconductivity. This concept is based on the idea that, under specific conditions, two electrons in a superconductor can form a bound pair, overcoming their natural electrostatic repulsion. The formation of Cooper pairs is governed by the Pauli exclusion principle, requiring the total wave function to be antisymmetric under particle exchange. This formation is possible through an interaction mediated by phonons, which are quasiparticles representing the vibrations of the crystal lattice in a solid. Physically, Cooper pairs are composed of two electrons with opposite momenta and spins that, when coupled, can move together through the conductor without resistance, a key feature of superconductivity.

In Cooper's work [43], it is shown that Cooper pairs have a slightly lower energy than individual electrons in the Fermi sea. This means that the normal state, where electrons are uncoupled, becomes "unstable" in the sense that a lower energy configuration is available, this is known as Cooper instability. In the following section, we will explain how Cooper pairs are related to the BCS theory.

2.3.2 BCS Hamiltonian

We will present the BCS Hamiltonian and subsequently diagonalize it using the Bogoliubov transformation. The BCS Hamiltonian, expressed in second quantization [44], is

$$H_{BCS} = \sum_{\mathbf{k}\sigma} \varepsilon_{\mathbf{k}} c^{\dagger}_{\mathbf{k}\sigma} c_{\mathbf{k}\sigma} + \sum_{\mathbf{k}\mathbf{k}'} V_{\mathbf{k}\mathbf{k}'} c^{\dagger}_{\mathbf{k}\uparrow} c^{\dagger}_{-\mathbf{k}\downarrow} c_{-\mathbf{k}'\downarrow} c_{\mathbf{k}'\uparrow}, \tag{2-7}$$

where $\varepsilon_{\mathbf{k}}$ is the dispersion energy, $V_{\mathbf{k}\mathbf{k}'}$ is the effective interaction potential between two electrons, $c^{\dagger}_{k\sigma}$ ($c_{k\sigma}$) creates (annihilates) an electron with momentum $\mathbf{k}$ and spin σ. Now we are going to apply mean-field theory to decouple the quartic operator and be able to diagonalize the Hamiltonian, obtaining

$$H^{MF}_{BCS} = \sum_{\mathbf{k}\sigma} \varepsilon_{\mathbf{k}} c^{\dagger}_{\mathbf{k}\sigma} c_{\mathbf{k}\sigma} + \sum_{\mathbf{k}} \Delta_{\mathbf{k}} c^{\dagger}_{\mathbf{k}\uparrow} c^{\dagger}_{-\mathbf{k}\downarrow} - \sum_{\mathbf{k}} \Delta_{\mathbf{k}} c_{-\mathbf{k}\downarrow} c_{\mathbf{k}\uparrow}, \tag{2-8}$$

where we can define the superconducting gap, which characterizes the superconducting state, as given by the following equation

$$\Delta_{\mathbf{k}} = -\sum_{\mathbf{k}'} V_{\mathbf{k}\mathbf{k}'} \langle c_{-\mathbf{k}'\downarrow} c_{\mathbf{k}'\uparrow} \rangle. \tag{2-9}$$

Now we will show one way to diagonalize this Hamiltonian using the Bogoliubov transformation. This transformation involves the introduction of new fermionic operators $\gamma^\dagger$ and γ, which correspond to the creation and destruction, respectively, of Bogoliubov quasiparticles. The matrix form of this transformation is expressed as follows

$$\begin{pmatrix} c_{\mathbf{k}\uparrow} \\ c^\dagger_{-\mathbf{k}\downarrow} \end{pmatrix} = \begin{pmatrix} u_{\mathbf{k}} & v_{\mathbf{k}} \\ -v^*_{\mathbf{k}} & u^*_{\mathbf{k}} \end{pmatrix} \begin{pmatrix} \gamma_{\mathbf{k}\uparrow} \\ \gamma^\dagger_{-\mathbf{k}\downarrow} \end{pmatrix}, \tag{2-10}$$

this unitary transformation is called the Bogoliubov-Valatin transformation. After substituting this transformation into the mean-field BCS Hamiltonian, it can be diagonalized if $u_{\mathbf{k}}$ and $v_{\mathbf{k}}$ have the following values

$$|u_{\mathbf{k}}|^2 = \frac{1}{2}\left(1 + \frac{\xi_{\mathbf{k}}}{E_{\mathbf{k}}}\right) \quad \text{and} \quad |v_{\mathbf{k}}|^2 = \frac{1}{2}\left(1 - \frac{\xi_{\mathbf{k}}}{E_{\mathbf{k}}}\right), \tag{2-11}$$

where $E_{\mathbf{k}} = \sqrt{\xi^2_{\mathbf{k}} + \Delta^2_{\mathbf{k}}}$. There is no loss of generality in choosing $u_{\mathbf{k}}$ to be real and positive, so we can express the Bogoliubov coefficients as follows

$$u_{\mathbf{k}} = \sqrt{\frac{1}{2}\left(1 + \frac{\xi_{\mathbf{k}}}{E_{\mathbf{k}}}\right)} \quad \text{and} \quad v_k = \mathrm{Sgn}(\Delta_{\mathbf{k}})\sqrt{\frac{1}{2}\left(1 - \frac{\xi_{\mathbf{k}}}{E_{\mathbf{k}}}\right)}, \tag{2-12}$$

where $u_{\mathbf{k}}$ and $v_{\mathbf{k}}$ satisfy the following relation: $u_{\mathbf{k}} v_{\mathbf{k}} = \Delta_{\mathbf{k}}/2E_{\mathbf{k}}$. After applying this transformation, we obtain the following Hamiltonian, ignoring the constant term.

After this transformation, we obtain (ignoring the constant term) the following Hamiltonian

$$H^{MF}_{BCS} = \sum_{\mathbf{k}} E_{\mathbf{k}} \left(\gamma^\dagger_{\mathbf{k}\uparrow}\gamma_{\mathbf{k}\uparrow} + \gamma^\dagger_{\mathbf{k}\downarrow}\gamma_{\mathbf{k}\downarrow}\right), \tag{2-13}$$

these quasiparticles are called Bogoliubons in honor of the Bogoliubov transformation that generates them. The Hamiltonian eq. (2-13) shows that the excited states of the BCS Hamiltonian are non-interacting fermionic excitations with energy $E_{\mathbf{k}}$ [45].

On the other hand, to calculate the superconducting gap, we use the Bogoliubov transformation in the definition of the superconducting gap given in eq. (2-9), obtaining the following expression

$$\Delta_{\mathbf{k}} = -\sum_{\mathbf{k}'} V_{\mathbf{k}\mathbf{k}'} \frac{\Delta_{\mathbf{k}'}}{2E_{\mathbf{k}'}} \left[1 - 2n_F(E_{\mathbf{k}'})\right], \tag{2-14}$$

where $n_F(E_{k'})$ is the Fermi-Dirac distribution. Bogoliubons are free fermions and therefore their distribution function follows the Fermi-Dirac distribution.

The eq. (2-14) is called the gap equation and characterizes the superconducting state since when $\Delta = 0$ it describes the normal state, whereas when $\Delta \neq 0$ we are in a superconducting state.

Next, we will describe some relevant equations of the BCS theory. First, if we take the ratio between the gap at zero temperature Δ_0 and the critical temperature T_c, the value is approximately [46].

$$\frac{2\Delta_0}{k_B T_c} \approx 3.528, \tag{2-15}$$

where k_B is the Boltzmann constant. This is a distinctive feature of the BCS theory, used experimentally to determine if a superconductor can be considered within the framework of this theory.

Another relevant equation known in the BCS theory is the one related to the coherence length, whose definition given by this theory is as follows [46]

$$\xi = \frac{\hbar v_F}{\pi \Delta_0}, \tag{2-16}$$

where v_F is the Fermi velocity and Δ is the superconducting gap. This quantity represents the spatial extension of a Cooper pair. For conventional superconductors, the coherence length is on the order of 100 nm, which is greater than the average distance between two electrons in a metal, meaning physically there is a huge overlap between Cooper pairs [45, 47].

After discussing BCS theory and presenting some relevant equations, in the following section, we will talk about singlet superconductors.

2.4 Singlet superconductors

Having reviewed BCS theory, now we will briefly comment on singlet superconductors. In this type of superconductors, the spins of the two electrons in the Cooper pair are antiparallel, so the total spin is zero. This differs from triplet superconductors, where the spins are parallel. Among singlet superconductors, we can find s-wave and d-wave superconductors, where we refer to the orbital symmetry of the Cooper pair's wave function. Now we will mention some characteristics of these types of superconductors.

First, we will begin with s-wave superconductors, which are very well described by the BCS theory. The superconducting gap they exhibit has isotropic symmetry, which means its value is the same in all directions in momentum space. This means that the Cooper pairs have zero angular momentum and therefore have spherical symmetry. On the other hand, d-wave superconductors have a superconducting gap that varies angularly, having points in momentum space where its value is zero; these points are called nodes.

This type of superconductors is characteristic of high-T_c superconductors [48, 49], among them, those based on copper oxide (cuprate superconductors).

In the following, we will show the notation we will use for some parameters of singlet superconductors in the dissertation. We will begin by expressing the single-particle Hamiltonian of a mean field spin-singlet superconductor as a Dirac Hamiltonian. To do this, we will start start from eq. (2-8) and express it in its matrix form using $|\psi_{\mathbf{k}}\rangle = \left(c^{\dagger}_{\mathbf{k}\uparrow}, c_{-\mathbf{k}\downarrow}\right)^{\dagger}$, which is called the Nambu basis

$$H^{MF}_{BCS} = (c^{\dagger}_{\mathbf{k}\uparrow}, c_{-\mathbf{k}\downarrow}) \begin{pmatrix} \varepsilon_k & \Delta_k \\ \Delta_k & -\varepsilon_k \end{pmatrix} \begin{pmatrix} c_{\mathbf{k}\uparrow} \\ c^{\dagger}_{-\mathbf{k}\downarrow \cdot} \end{pmatrix}, \tag{2-17}$$

where the single-particle Hamiltonian is represented by

$$H(\mathbf{k}) = \begin{pmatrix} \varepsilon_k & \Delta_k \\ \Delta_k & -\varepsilon_k \end{pmatrix}. \tag{2-18}$$

We may represent this Hamiltonian as a 2×2 Dirac Hamiltonian

$$H(\mathbf{k}) = \mathbf{d}.\boldsymbol{\sigma} = d_1\sigma_1 + d_3\sigma_3, \tag{2-19}$$

where σ_i are the Pauli matrices, $d_1 = \Delta_{\mathbf{k}}$ is the momentum dependent superconducting gap, and $d_3 = \varepsilon_{\mathbf{k}}$ is the normal state dispersion. Now we proceed to define a unit vector

$$\mathbf{n} \equiv \mathbf{d}/|\mathbf{d}| = (d_1/d, d_3/d) = (n_1, n_3)\,, \tag{2-20}$$

where $\pm d = \pm\sqrt{d_1^2 + d_3^2} = \pm E_{\mathbf{k}}$. After diagonalizing eq. (2-19) we find that the filled quasihole eigenstate given by $|n(\mathbf{k})\rangle \equiv |n\rangle$ with eigenenergy $-E_{\mathbf{k}}$ and the empty quasiparticle eigenstate $|m(\mathbf{k})\rangle \equiv |m\rangle$ with eigenenergy $+E_{\mathbf{k}}$ are expressed in the following way

$$|n\rangle = \frac{1}{\sqrt{2d(d-d_3)}} \begin{pmatrix} d - d_3 \\ -d_1 \end{pmatrix} = \mathrm{Sgn}(\Delta_{\mathbf{k}}) \begin{pmatrix} v_k \\ -u_k \end{pmatrix}, \tag{2-21}$$

$$|m\rangle = \frac{1}{\sqrt{2d(d+d_3)}} \begin{pmatrix} d + d_3 \\ d_1 \end{pmatrix} = \begin{pmatrix} u_k \\ v_k \end{pmatrix}, \tag{2-22}$$

where $u_{\mathbf{k}}$ and $v_{\mathbf{k}}$ are the Bogoliubov coefficients eq. (2-12). For the study of the quantum geometry of singlet superconductors, we have expressed the single-particle Hamiltonian of the mean field spin-singlet superconductors in the form of a 2×2 Dirac Hamiltonian. This was done because it is possible to use some definitions of quantum metric for Hamiltonians that can be expressed in the form of a Dirac Hamiltonian [16], as we will see in the next chapter.

3
Quantum geometry of singlet superconductors

In this chapter, we will review some quantities of quantum geometry such as the quantum metric, the fidelity number, and the fidelity marker, to subsequently focus on studying these quantities for singlet superconductors. Additionally, we present a way to visualize this metric using a vector whose components are the Bogoliubov coefficients. We find that for s-wave superconductors, their quantum metric is nontrivial. Furthermore, we express this metric and the fidelity number analytically using a continuous model that will be detailed in appendix C and observe the influence of impurities on the quantum geometry through the fidelity marker. For the case of d-wave superconductors, we observe that their metric around the nodal points diverges, leading to a divergence in their fidelity number as well.

3.1
Quantum geometry

The investigation of quantum geometry may be characterized by the quantum geometric tensor [50, 51]. This quantity is derived by computing the distance between two proximate states $|\psi(k)\rangle$ and $|\psi(k+\delta k)\rangle$ situated in momentum space, as shown below

$$ds^2 = 1 - |\langle\psi(\mathbf{k})|\psi(\mathbf{k}+\delta\mathbf{k})\rangle|^2, \tag{3-1}$$

the ds^2 term is consistently positive, hence the Taylor expansion about $\delta\mathbf{k} = 0$ lacks any first-order terms and begins with the quadratic term

$$ds^2 = \sum_{\mu\nu} T_{\mu\nu}\delta k^\mu \delta k^\nu, \tag{3-2}$$

where $T_{\mu\nu}$ is the quantum metric tensor, which can be defined as follows

$$T_{\mu\nu} = \langle\partial_\mu\psi|\partial_\nu\psi\rangle - \langle\partial_\mu\psi|\psi\rangle\langle\psi|\partial_\nu\psi\rangle, \tag{3-3}$$

where $\partial_\mu = \partial/\partial k^\mu$. This quantum metric tensor can be reformulated as [52]

$$T_{\mu\nu} = g_{\mu\nu} - \frac{i}{2}F_{\mu\nu}, \tag{3-4}$$

the terms $g_{\mu\nu}$ and $F_{\mu\nu}$ represent the quantum metric and the Berry curvature, respectively, and they can be articulated as follows

$$g_{\mu\nu} = \frac{1}{2}\langle\partial_\mu\psi|\partial_\nu\psi\rangle + \frac{1}{2}\langle\partial_\nu\psi|\partial_\mu\psi\rangle - \langle\partial_\mu\psi|\psi\rangle\langle\psi|\partial_\nu\psi\rangle, \tag{3-5}$$

$$F_{\mu\nu} = i\langle\partial_\mu\psi|\partial_\nu\psi\rangle - i\langle\partial_\nu\psi|\partial_\mu\psi\rangle. \tag{3-6}$$

Since $g_{\mu\nu}$ represents the real part of $T_{\mu\nu}$ and $F_{\mu\nu} = -F_{\nu\mu}$, we can use equations eqs. (3-1) and (3-2) to arrive at the following definition for the quantum metric

$$|\langle\psi(\mathbf{k})|\psi(\mathbf{k}+\delta\mathbf{k})\rangle| = 1 - \frac{1}{2}g_{\mu\nu}\delta k^\mu \delta k^\nu. \tag{3-7}$$

The eq. (3-7) indicates that if we take the modulus of a state $|\psi(\mathbf{k})\rangle$ that overlaps with itself at slightly different momenta and perform an expansion in terms of small displacement $\delta\mathbf{k}$, the result introduces a prefactor called $g_{\mu\nu}$, which is the quantum metric. A very intuitive picture that allows us to visualize this is fig. 3.1, where we have the unit vector $|\psi(\mathbf{k})\rangle$ in the Hilbert space in some basis $|n_1\rangle$, $|n_2\rangle$, and $|n_3\rangle$. This vector is pointing in some direction, and when we move from $\mathbf{k}$ to $\mathbf{k}+\delta\mathbf{k}$, this unit vector will rotate to a different direction in the Hilbert space. If we now take the product between these two unit vectors, the result must be less than one. Hence, if an expansion is performed, the correction should give us the quantum metric.

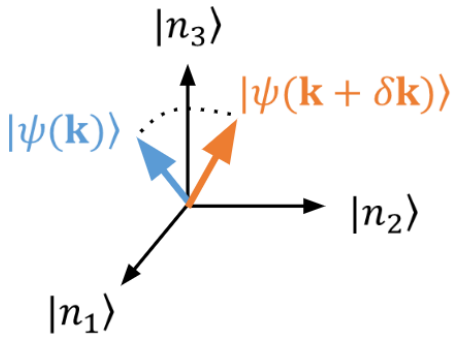

Figure 3.1: Representation of how a unit vector $|\psi(\mathbf{k})\rangle$ in the Hilbert space in some basis $|n_1\rangle$, $|n_2\rangle$, and $|n_3\rangle$ rotates as we move from $\mathbf{k}$ to $\mathbf{k}+\delta\mathbf{k}$. This Figure was created by the author.

Now we will demonstrate the calculation of the quantum metric in systems that have a band gap, such as insulating or superconducting systems. We will use n for valence bands, m for conduction bands, and l for all bands. The Bloch states of each band are expressed as [15, 53]

$$|l^{\mathbf{k}}\rangle = \sum_{\mathbf{R}} e^{-i\mathbf{k}\cdot(\mathbf{r}-\hat{\mathbf{R}})}|\mathbf{R}l\rangle, \tag{3-8}$$

$$|\mathbf{R}l\rangle = \sum_{\mathbf{k}} e^{i\mathbf{k}\cdot(\hat{\mathbf{r}}-\mathbf{R})}|l^{\mathbf{k}}\rangle, \tag{3-9}$$

where the wavefunctions in the position r are denoted by $\langle\mathbf{r}|\mathbf{R}n\rangle = W_n(\mathbf{r}-\mathbf{R})$, which correspond to Wannier functions that are highly localized around the

home cell **R**.

We assume that N_- (N_+) are the Bloch functions of occupied (unoccupied) states for each **k**. In this case, the fully antisymmetric valence-band Bloch state at momentum **k** is

$$|u^{val}(k)\rangle = \frac{1}{\sqrt{N_-!}} e^{n_{a_1} n_{a_2} \ldots n_{a_{N_-}} k} |n^k_{a_1}\rangle |n^k_{a_2}\rangle \ldots |n^k_{a_{N_-}}\rangle, \tag{3-10}$$

where $|n^k_a\rangle$ forms a basis for the N_- filled bands. Now we will proceed to study the quantum metric of this state $|u^{val}(k)\rangle$ using the definition given in eq. (3-7), we have

$$|\langle u^{val}(\mathbf{k})|u^{val}(\mathbf{k}+\delta\mathbf{k})\rangle| = 1 - \frac{1}{2} g_{\mu\nu}\delta k^\mu \delta k^\nu. \tag{3-11}$$

Then, we can express the metric in the following way

$$g_{\mu\nu} = \frac{1}{2}\langle \partial_\mu u^{val}|\partial_\nu u^{val}\rangle + \frac{1}{2}\langle \partial_\nu u^{val}|\partial_\mu u^{val}\rangle - \langle \partial_\mu u^{val}|u^{val}\rangle\langle u^{val}|\partial_\nu u^{val}\rangle. \tag{3-12}$$

It is possible to express this metric in terms of one-particle states [16]

$$g_{\mu\nu}(k) = \frac{1}{2}\sum_a \left(\langle \partial_\mu u_a|Q_+|\partial_\nu u_a\rangle + \langle \partial_\mu u_a|Q_+|\partial_\nu u_a\rangle\right), \tag{3-13}$$

where Q_+ (Q_-) is the projector on the positive (negative) eigenstates

$$Q_\pm \equiv \sum_{a=1}^{N_\pm} |u^\pm_a\rangle\langle u^\pm_a|, \tag{3-14}$$

which satisfy that $Q_+ + Q_- = 1$. Physically, eq. (3-12) measures how much the state $|u^{val}\rangle$ has rotated from momentum **k** to $\mathbf{k}+\delta\mathbf{k}$ in the Hilbert space of N_--particles.

3.1.1 Fidelity number

Another relevant geometric quantity is the fidelity number. Before defining it, it is crucial to mention that the Brillouin zone in a dimension D can be considered as a toroid T^D from a differential geometry perspective. Then, it can be inferred that by integrating the quantum metric over momentum space on the toroid T^D

$$\mathcal{G}_{\mu\nu} = \int \frac{d^D\mathbf{k}}{(2\pi)^D} g_{\mu\nu}(\mathbf{k}), \tag{3-15}$$

represents the average distance between neighboring Bloch states, $|\psi(\mathbf{k})\rangle$ and $|\psi(\mathbf{k}+\delta\mathbf{k})\rangle$; this new quantity may be considered an intrinsic property of the quantum geometry, and is referred to as the fidelity number [15].

3.1.2 Fidelity marker

Now, we will briefly demonstrate how we can map the fidelity number onto the lattice sites in real space [15]. Starting from the definition of the fidelity number and using the defined metric, we can obtain the following relationship.

$$\mathcal{G}_{\mu\nu} = \frac{1}{2\hbar^2}\int \frac{d^D\mathbf{k}}{(2\pi)^D}\langle\psi_{n\mathbf{k}}|\hat{\mu}|\psi_{m\mathbf{k}}\rangle\langle\psi_{m\mathbf{k}}|\hat{\nu}|\psi_{n\mathbf{k}}\rangle + (\mu \leftrightarrow \nu),$$
$$\mathcal{G}_{\mu\nu} = \frac{\hbar^{D-2}}{2a^D}\int \frac{d^D\mathbf{k}}{(2\pi)^D}\frac{d^D\mathbf{k}'}{(2\pi)^D}\langle\psi_{n\mathbf{k}}|\hat{\mu}|\psi_{m\mathbf{k}'}\rangle\langle\psi_{m\mathbf{k}'}|\hat{\nu}|\psi_{n\mathbf{k}}\rangle + (\mu \leftrightarrow \nu), \quad (3\text{-}16)$$

in which $\langle r|\psi_{n\mathbf{k}}\rangle = e^{i\mathbf{k}\cdot\mathbf{r}/\hbar}\langle\mathbf{r}|n(\mathbf{k})\rangle$ is the full quasihole state wave function (and likewise for $|m(\mathbf{k})\rangle$), and we have employed the following identity [54, 55]

$$i\langle m|\partial_\mu n\rangle = \frac{1}{\hbar}\langle\psi_{m\mathbf{k}}|\hat{\mu}|\psi_{n\mathbf{k}'}\rangle. \quad (3\text{-}17)$$

Returning to eq. (3-16), we can observe that it may be related to the projection operators of the valence and conduction band states, given, respectively, as

$$\hat{P} = \sum_n \int \frac{d^D\mathbf{k}}{(2\pi)^D}|\psi_{n\mathbf{k}}\rangle\langle\psi_{n\mathbf{k}}|, \quad (3\text{-}18)$$
$$\hat{Q} = \sum_m \int \frac{d^D\mathbf{k}'}{(2\pi)^D}|\psi_{m\mathbf{k}'}\rangle\langle\psi_{m\mathbf{k}'}|. \quad (3\text{-}19)$$

Now considering a tight-binding Hamiltonian expressed in second quantization $H = \sum_{\mathbf{r}\mathbf{r}'\sigma\sigma'} t_{\mathbf{r}\mathbf{r}'\sigma\sigma'}c^\dagger_{\mathbf{r}\sigma}c_{\mathbf{r}'\sigma'}$, where t is the hopping term and $\mathbf{r}$ labels the lattice sites. We proceed with the diagonalization of this Hamiltonian $H|E_l\rangle = E_l|E_l\rangle$, thereby obtaining the eigenstates $|E_l\rangle$ along with the corresponding eigenvalues E_l. Proceeding with an analogous definition of projectors, defined in eqs. (3-18) and (3-19), we can define the projectors using the eigenstates $|E_l\rangle$ as follows

$$\hat{P} = \sum_n |E_n\rangle\langle E_n|, \quad (3\text{-}20)$$
$$\hat{Q} = \sum_m |E_m\rangle\langle E_m|. \quad (3\text{-}21)$$

Using these projectors, we can be reformulated the fidelity number as

$$\mathcal{G}_{\mu\nu} = \frac{1}{2}Tr\left[\hat{P}\,\hat{r}_\mu\,\hat{Q}\,\hat{r}_\nu\hat{P} + (\mu \leftrightarrow \nu)\right], \quad (3\text{-}22)$$

$$\mathcal{G}_{\mu\nu} = \frac{1}{N}\sum_{\mathbf{r}}\mathcal{G}_{\mu\nu}(\mathbf{r}), \quad (3\text{-}23)$$

where $\hat{r}_\mu$ and $\hat{r}_\nu$ represent the position operators on the lattice. The trace in this expression is taken over the lattice sites $\mathbf{r}$, and each term in the summation delineates what we will refer to as the fidelity marker

$$\mathcal{G}_{\mu\nu}(\mathbf{r}) \equiv \frac{\hbar^{D-2}}{2a^D}\langle\mathbf{r}|\left[\hat{P}\,\hat{r}_\mu\,\hat{Q}\,\hat{r}_\nu\,\hat{P} + \hat{P}\,\hat{r}_\nu\,\hat{Q}\,\hat{r}_\mu\,\hat{P}\right]|\mathbf{r}\rangle. \tag{3-24}$$

The relevance of this last equation is that, by being the projection of the fidelity number at each site of the lattice, we can obtain information about the average distance between neighboring quasihole states $|n(\mathbf{k})\rangle$ and $|n(\mathbf{k}+\delta\mathbf{k})\rangle$ in real space. In the following sections, we shall see how the fidelity marker can be used to characterize the influence of real space inhomogeneity on the quantum geometry.

3.2 Quantum geometry of s-wave superconductors

Having reviewed quantum geometry, we now focus first on the quantum metric $g_{\mu\nu}(\mathbf{k})$ of the filled quasihole state $|n(\mathbf{k})\rangle$ of s-wave superconductors. Using the expression eq. (3-7) for the filled quasihole state, we obtain the following equation

$$|\langle n(\mathbf{k})|n(\mathbf{k}+\delta\mathbf{k})\rangle| = 1 - \frac{1}{2}g_{\mu\nu}\delta k^\mu \delta k^\nu. \tag{3-25}$$

Now, using the definition given in eq. (3-13) applied to this type of superconductors we have that the metric can be expressed in the following way

$$g_{\mu\nu}(\mathbf{k}) = \frac{1}{2}\left[\langle\partial_\mu n|m\rangle\langle m|\partial_\nu n\rangle + \langle\partial_\nu n|m\rangle\langle m|\partial_\mu n\rangle\right], \tag{3-26}$$

using the expressions eqs. (2-21) and (2-22) in eq. (3-26), we arrive at the following expression

$$g_{\mu\nu}(\mathbf{k}) = (u_\mathbf{k}\partial_\mu v_\mathbf{k} - v_\mathbf{k}\partial_\mu u_\mathbf{k})(u_\mathbf{k}\partial_\nu v_\mathbf{k} - v_\mathbf{k}\partial_\nu u_\mathbf{k}). \tag{3-27}$$

Now, because the single-particle Hamiltonian of singlet superconductors can be expressed as a Dirac Hamiltonian, we can have another equivalent expression for the quantum metric [16] which is

$$g_{\mu\nu} = \frac{1}{4}\partial_\mu\mathbf{n}\cdot\partial_\nu\mathbf{n}, \tag{3-28}$$

where $\mathbf{n}$ is the unit vector given by eq. (2-20). Using the definition of this unit vector and after some algebra, we have

$$g_{\mu\nu} = \frac{1}{4d^4}(d_3\partial_\mu d_1 - d_1\partial_\mu d_3)(d_3\partial_\nu d_1 - d_1\partial_\nu d_3). \tag{3-29}$$

To calculate the quantum metric of singlet superconductors, both eq. (3-27) and eq. (3-29) can be used. Now we will focus on s-wave superconductors where

we have that $d_1 = \Delta$ is a constant and the derivative of the dispersion of the normal state is $\partial_\mu d_3 = \partial_\mu \varepsilon_{\mathbf{k}} = v_\mu(\mathbf{k}) \equiv v_\mu$ which is the group velocity of the normal state along the direction μ with momentum $\mathbf{k}$. Then, the quantum metric, using eq. (3-29), is

$$g_{\mu\nu} = \frac{\Delta^2 v_\mu v_\nu}{4E_{\mathbf{k}}^4}, \tag{3-30}$$

which represents the quantum metric of the filled quasihole state $|n(\mathbf{k})\rangle$ for s-wave superconductors. To visualize this metric, one can make use of its relationship with the Bogoliubov coefficients. This is because we define the quantum metric of the filled quasihole state, and this state is connected to the Bogoliubov coefficients as noted in eq. (2-21). Consequently, we define the unitary vector field in D-dimensional k-space as $\mathbf{w_k} = (v_{\mathbf{k}}, -u_{\mathbf{k}})$, where $v_{\mathbf{k}}$ and $-u_{\mathbf{k}}$ are the Bogoliubov coeffient

$$|\langle n(\mathbf{k})|n(\mathbf{k}+\delta\mathbf{k})\rangle| = |\mathbf{w_k} \cdot \mathbf{w_{k+\delta k}}|. \tag{3-31}$$

By substituting eq. (3-31) into eq. (3-25), we obtain

$$\frac{1}{2} g_{\mu\nu} \delta k^\mu \delta k^\nu = 1 - |\mathbf{w_k} \cdot \mathbf{w_{k+\delta k}}|. \tag{3-32}$$

The equation above indicates that as the product $|\mathbf{w_k} \cdot \mathbf{w_{k+\delta k}}|$ deviates further from unity, the metric's value increases. Alternatively, this can be understood in terms of how much the unit vector in the Hilbert space $\mathbf{w_k}$ "twists" when transitioning from $\mathbf{k}$ to $\mathbf{k} + \delta\mathbf{k}$.

To show the results obtained from the quantum metric, we will consider the dispersion energy of a D-dimensional cubic lattice using a tight-binding model [56] with nearest-neighbor hopping t and chemical potential μ expressed in the following way

$$\varepsilon_{\mathbf{k}} = -2t \sum_{i=1}^{D} \cos k_i - \mu. \tag{3-33}$$

Then, to calculate the quantum metric g_{xx} for a lattice in 2D and 3D, we will use eq. (3-30) and will set the hopping $t = 1$, the chemical potential $\mu = -0.2t$, and the gap $\Delta = 0.5t$, we have used these values solely for the purpose of visualizing the shape of the quantum metric, obtaining as a result the figs. 3.2 and 3.3 which will be described below.

In fig. 3.2 (a), we show the vector field of $\mathbf{w_k} = (v_{\mathbf{k}}, -u_{\mathbf{k}})$ defined using the Bogoliubov coefficients, as discussed in section 3.2, in 2D. We can observe that near the Fermi surface (red dashed line in fig. 3.2 (b)), this vector field has a very strong twisting. This is because below the Fermi surface, the eigenstates are predominantly electronlike, and above the Fermi surface, they are predominantly holelike, resulting in a strong twisting at the Fermi surface. Correspondingly, as observed in fig. 3.2 (a), we see a huge quantum metric g_{xx} at the Fermi surface in fig. 3.2 (b). It should also be noted that both figures

show the first quadrant of the Brillouin zone.

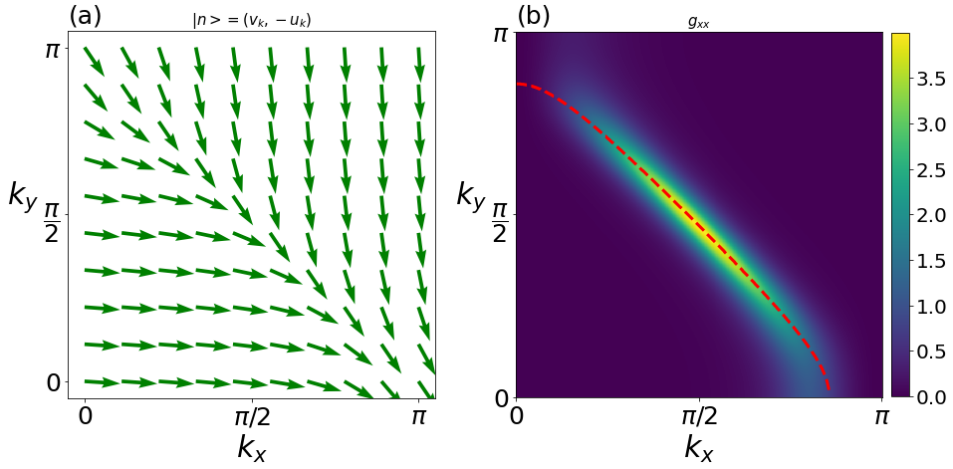

Figure 3.2: In (a), the vector field given by the vector $\mathbf{w} = (v_{\mathbf{k}}, -u_{\mathbf{k}})$ for a 2D s-wave superconductor in the first quarter of the Brillouin zone is shown. We observe that the region where this vector changes its direction indicates the region where the quantum metric g_{xx} is different from zero as seen in (b). Additionally, we observe that the metric reaches its maximum near the Fermi surface (dashed line). This Figure has been taken from Ref. [57].

In a manner equivalent to the 2D case, in fig. 3.3(a) we show the vector field of $\mathbf{w_k} = (v_{\mathbf{k}}, -u_{\mathbf{k}})$ in 3D where, for better visualization, only the vector field for $k_z = 0, \pi/2, \pi$ has been chosen. We see that the behavior is the same as in the 2D case because the regions where the vector field changes direction are the same where g_{xx} shows a peak in its value fig. 3.3(b).

In conclusion, these two figs. 3.2 and 3.3 illustrate the shape of the quantum metric for s-wave superconductors, as well as a way to visualize this metric through a vector $\mathbf{w_k} = (v_{\mathbf{k}}, -u_{\mathbf{k}})$ formed with the Bogoliubov coefficients.

3.2.1 Fidelity number of s-wave superconductors

For the 2D case, the calculations to obtain the analytical expression of $G^{2D}_{\mu\mu}$ are shown in appendix C, here we will only show the final expression

$$\mathcal{G}^{2D}_{\mu\mu} = \int \frac{d^2\mathbf{k}}{(2\pi)^2} g_{\mu\mu}, \tag{3-34}$$

$$\mathcal{G}^{2D}_{\mu\mu} = \frac{\pi^2}{8\sqrt{2}} \left(\frac{\xi}{a}\right) \left(\frac{k_F}{2\pi\hbar/a}\right), \tag{3-35}$$

where we see that it is a dimensionless number, the expression $k_F/(2\pi\hbar/a)$ is of the order of unity so the relevant part is represented by the coherence length divided by the lattice constant ξ/a.

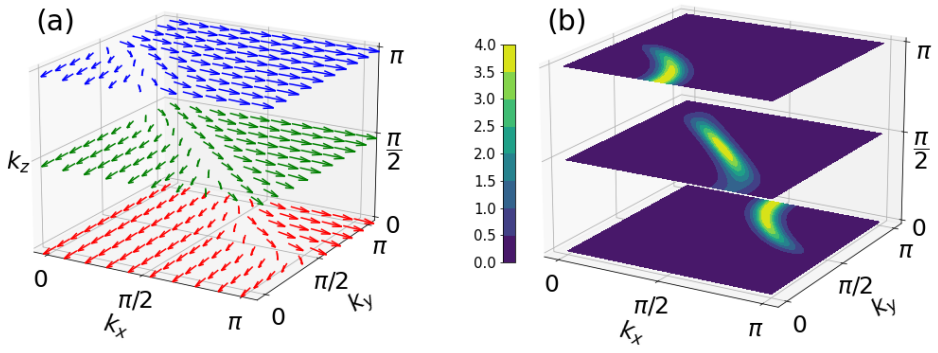

Figure 3.3: (a) Shows the vector field of the vector $\mathbf{w} = (v_{\mathbf{k}}, -u_{\mathbf{k}})$ for $k_z = 0, \pi/2, \pi$, in order to have a better visualization, where we observe the same behavior as in the 2D case. This is because the regions where the vector $\mathbf{w}$ changes direction are the regions where the quantum metric reaches its maximum as shown in (b). This Figure has been taken from Ref. [57].

On the other hand, for the 3D case, we have that its analytical expression is derived in appendix C, we will only show here its final expression which is

$$\mathcal{G}^{3D}_{\mu\mu} = \int \frac{d^3\mathbf{k}}{(2\pi)^3} g_{\mu\mu}, \tag{3-36}$$

$$\mathcal{G}^{3D}_{\mu\mu} = \frac{\pi^2}{6\sqrt{2}} \left(\frac{\xi}{a}\right) \left(\frac{k_F}{2\pi\hbar/a}\right)^2 \left(\frac{\hbar}{a}\right), \tag{3-37}$$

this last expression tells us that the fidelity number in 3D depends to a greater extent on the coherence length divided by the lattice constant ξ/a times $\hbar/a$ since the expression $k_F/(2\pi\hbar/a)$ is of the order of unity.

Thus, we observe that the fidelity number for s-wave superconductors in 2D and 3D, given by eqs. (3-35) and (3-37), is directly related to the coherence length. Consequently, we can arrive at two very important conclusions. The first is that we can have another interpretation of the coherence length within quantum geometry, which can be understood as the measure of the average distance between neighboring quasihole states across the entire Brillouin zone. The second is that if any property in this type of superconductors is related to the coherence length, then it can also be related to the fidelity number.

3.2.2 Fidelity marker of s-wave superconductors

Now, we will proceed to study the effect of a nonmagnetic impurity on the fidelity marker in s-wave superconductors. For the calculation of the fidelity marker, similarly to what was explained in section 3.1.2, we first consider a lattice Bogoliubov-de Gennes (BdG) Hamiltonian H_{BdG}. Then, we consider a

nonmagnetic on-site impurity U, which we place at the center of the lattice to observe how the fidelity marker is locally modified. We proceed to diagonalize the Hamiltonian with the on-site impurity $H|E_l\rangle = E_l|E_l\rangle$, obtaining the filled $E_n < 0$ and empty $E_m > 0$ lattice eigenstates. Now, using these eigenstates to construct the projectors in eqs. (3-20) and (3-21) and subsequently using eq. (3-24), we can calculate the fidelity marker for s-wave superconductors.

Next, we will show the results obtained for the effect of the impurity on the fidelity marker in s-wave superconductors in both 2D and 3D. For the 2D case, we have fig. 3.4, where fig. 3.4(a) shows the fidelity marker at each site of a square lattice, where a nonmagnetic impurity $U = 2t$ has been placed at the center of the lattice. Meanwhile, for fig. 3.4(b), a nonmagnetic impurity $U = 1000t$ has been considered. We observe that by increasing the value of the nonmagnetic impurity, the fidelity marker locally decreases.

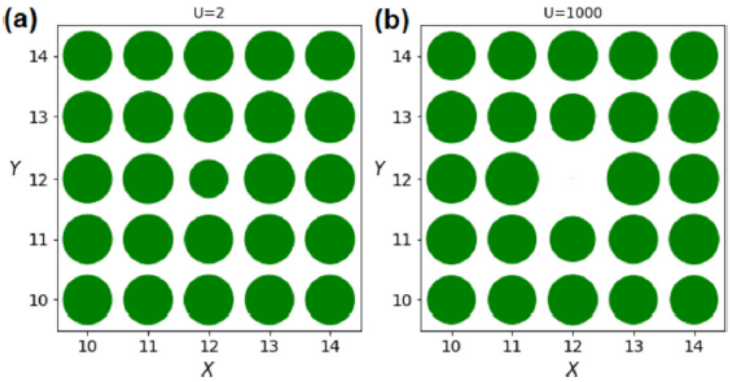

Figure 3.4: (a) Shows the fidelity marker for a 2D s-wave superconductor, where a nonmagnetic impurity has been introduced at the center of the lattice with $U = 2t$, observing that the largest circle represents a magnitude of 0.433 and that the marker decreases due to the impurity. For (b), a nonmagnetic impurity with $U = 1000t$ has been considered; in this case, the largest circle corresponds to a value of 0.474, where we observe that due to the value of the impurity, the fidelity marker is practically zero. This Figure has been taken from Ref. [57].

On the other hand, we have the 3D case, which is depicted by fig. 3.5. Here, fig. 3.5(a) shows the fidelity marker at each site of a cubic lattice, where a nonmagnetic impurity $U = 2t$ has been introduced at the center of the lattice, while fig. 3.5(b) considers a scenario where a nonmagnetic impurity $U = 1000t$ has been introduced. We observe equivalent results to the 2D case, where we see that the nonmagnetic impurity decreases the fidelity marker locally. Physically, this indicates for both dimensions that this type of impurity reduces the average distance between quasihole states in momentum space.

We can conclude from what is observed in both figs. 3.4 and 3.5 that the nonmagnetic impurity locally suppresses the fidelity marker, indicating that

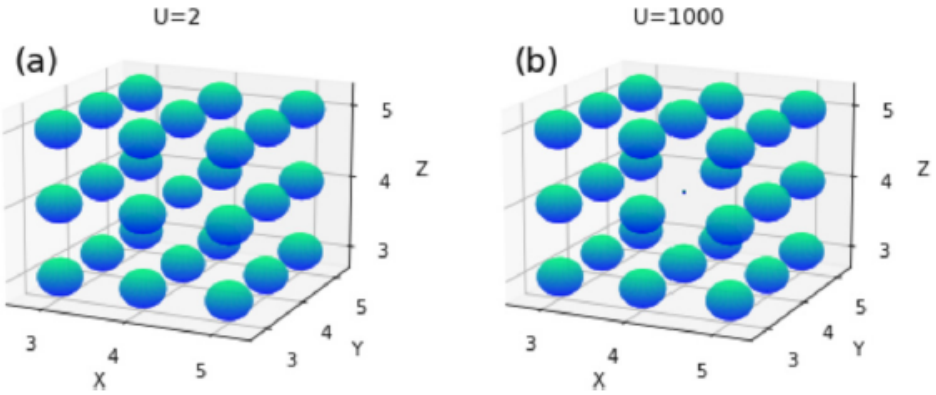

Figure 3.5: (a) Shows the fidelity marker for a 3D s-wave superconductor where a nonmagnetic impurity $U = 2t$ has been introduced, the largest sphere represents a value of 0.332. (b) In this case, a nonmagnetic impurity $U = 1000t$ was considered, and the largest sphere corresponds to 0.339. We observe that the results are equivalent to the 2D case, where the nonmagnetic impurity decreases the fidelity marker. This Figure has been taken from Ref. [57].

disorder affects the quantum geometry in this type of superconductors.

3.3 Quantum geometry of d-wave superconductors

In this section, we will study the quantum geometry of d-wave superconductors. For this type of superconductors, we will consider the framework of the BCS theory, using the mean-field theory, because some works related to cuprate superconductors indicate that we can make these considerations in certain regions of their phase diagram related to doping [58, 59, 60].

We will proceed in a similar manner to what we did for s-wave superconductors, calculating the quantum metric and the Bogoliubov coefficients for this type of superconductors. For the calculation of the quantum metric, we start from Equation 3-29, for the superconducting gap $d_1 = \Delta_k$ we will express it as [60]

$$\Delta_k = 2\Delta_0(\cos k_x - \cos k_y). \tag{3-38}$$

On the other hand, for the dispersion energy of the normal state $d_3 = \varepsilon_k$ we will use a tigh-binding model for a 2D lattice and in order to examine a more real system we will take into account second neighbors obtaining

$$\varepsilon_{\mathbf{k}} = -2t(\cos k_x + \cos k_y) + 4t' \cos k_x \cos k_y - \mu. \tag{3-39}$$

Replacing both the eqs. (3-38) and (3-39) into the eq. (3-29) we have the

quantum metric for d-wave superconductors having the following form

$$g_{\mu\nu} = e_\mu e_\nu, \tag{3-40}$$

$$e_x = \frac{\Delta_0}{E_k^2} \sin k_x \left(4t \cos k_y - 4t' \cos^2 k_y + \mu\right), \tag{3-41}$$

$$e_y = \frac{\Delta_0}{E_k^2} \sin k_y \left(-4t \cos k_x + 4t' \cos^2 k_x - \mu\right). \tag{3-42}$$

For the numerical calculation of the quantum metric, we will use the following parameter values (in units of eV): $t = 0.15$, $t' = 0.04$, and $\mu = -0.13$. These values are optimal for the optimally doped to slightly overdoped superconducting cuprate $Bi_2Sr_2CaCu_2O_{8+x}$ [60] and we use a larger value of the gap, $\Delta_0 = 0.1$, purely to demonstrate the momentum profile of the quantum metric.

For the case of the Bogoliubov coefficients of d-wave superconductors, we use the expressions previously shown in Equation eq. (2-12) and replace the dispersion energy of the normal state and the d-wave superconducting gap given by Equations eq. (3-38) and eq. (3-39), respectively.

Considering the equations and parameter values mentioned above, we obtain both fig. 3.6(a) and (b), which are both in the first quadrant of the Brillouin zone. In fig. 3.6(a), we show the vector field given by the unit vector (u_k, v_k), formed with the Bogoliubov coefficients, where we observe the formation of a vortex around the nodal point. As mentioned earlier, the vector $\mathbf{w_k}$ represents the quasihole state as a unit vector in Hilbert space, so the vortex indicates that the quasihole state rotates dramatically in Hilbert space around the nodal point. This is consistent with what is observed in fig. 3.6(b), which shows how a pair of maxima of the metric appear around the nodal point. For better visualization of these maxima, we restrict the value of the metric since its value diverges at the nodal point. Next, we will show how we can capture this divergence through its equation. To better visualize the profile of the quantum metric, we will make the following consideration $t' = \mu = 0$ where the nodal point is located at $k_0 = (\pi/2, \pi/2)$. Thus, an analytical expression for the quantum metric around the nodal point $\mathbf{k} = \mathbf{k}_0 + \delta\mathbf{k}$, which we will

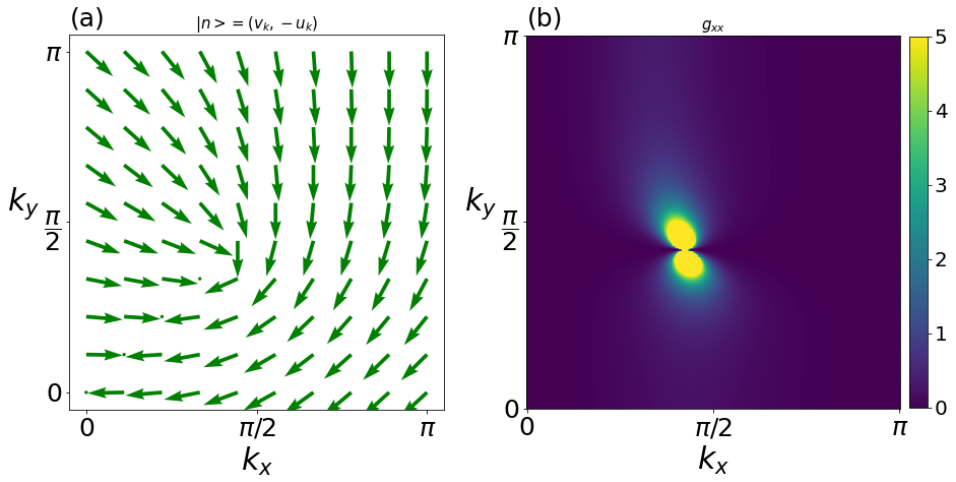

Figure 3.6: (a) The vector field of the vector $\mathbf{w_k}$ for d-wave superconductors in 2D in the first quarter of the Brillouin zone is shown. We can observe that the vectors form a vortex around the nodal point. This is consistent with what is observed in (b), where the quantum metric shows singular behavior at the nodal point, and two maxima appear around this point. This Figure has been taken from Ref. [57].

call the bare quantum metric $\overline{g}_{\mu\nu}$, has the following form:

$$\begin{aligned}
\overline{g}_{xx} &\approx \frac{\Delta_0^2 t^2 \delta k_y^2}{\left[(t^2+\Delta_0^2)(\delta k_x^2+\delta k_y^2)+2(t^2-\Delta_0^2)\delta k_x \delta k_y\right]^2}, \\
\overline{g}_{yy} &\approx \frac{\Delta_0^2 t^2 \delta k_x^2}{\left[(t^2+\Delta_0^2)(\delta k_x^2+\delta k_y^2)+2(t^2-\Delta_0^2)\delta k_x \delta k_y\right]^2}, \\
\overline{g}_{xy} &\approx \frac{-\Delta_0^2 t^2 \delta k_x \delta k_y}{\left[(t^2+\Delta_0^2)(\delta k_x^2+\delta k_y^2)+2(t^2-\Delta_0^2)\delta k_x \delta k_y\right]^2},
\end{aligned} \tag{3-43}$$

where we can observe in each of the equations that as we approach the nodal point in both directions $\delta k_x, \delta k_y \to 0$, their value diverges.

Next, we will calculate the fidelity number for d-wave superconductors. First, we will make a change to polar coordinates for the bare quantum metric, to subsequently perform an integration in polar coordinates which would help us observe the behavior of the fidelity number due to its definition in eq. (3-15). The bare quantum metric, given by section 3.3, making the change to polar

coordinates $(\delta k_x, \delta k_y) = (k\cos\theta, k\sin\theta)$ has the following form

$$\begin{aligned}
\overline{g}_{xx} &\approx \frac{1}{k^2} \times \frac{\Delta_0^2 t^2 \sin^2\theta}{\left[(t^2+\Delta_0^2) + (t^2-\Delta_0^2)\sin 2\theta\right]^2}, \\
\overline{g}_{yy} &\approx \frac{1}{k^2} \times \frac{\Delta_0^2 t^2 \cos^2\theta}{\left[(t^2+\Delta_0^2) + (t^2-\Delta_0^2)\sin 2\theta\right]^2}, \\
\overline{g}_{xy} &\approx \frac{1}{k^2} \times \frac{-\Delta_0^2 t^2 \sin\theta\cos\theta}{\left[(t^2+\Delta_0^2) + (t^2-\Delta_0^2)\sin 2\theta\right]^2},
\end{aligned} \tag{3-44}$$

where it is possible to notice that upon performing the polar integration, we see that the result diverges logarithmically. Therefore, for d-wave superconductors, we obtain that the fidelity number diverges, due to the behavior of the quantum metric around the nodal points, which physically indicates that the average distance between Bloch states in the Brillouin zone for this type of superconductors diverges.

4
Electromagnetic responses in singlet superconductors and their relationship with quantum geometry

In this chapter, we will study the electromagnetic responses for the case of singlet superconductors, demonstrating the relationship of these responses with quantum geometry for the case of s-wave superconductors. It is important to highlight that the calculations will be performed for both 2D and 3D lattices. Regarding the electromagnetic responses, we will analyze infrared absorption, paramagnetic current, and linear screening, obtaining such electromagnetic responses expressed in terms of coherence factors for the case of singlet superconductors. To study the relationship with quantum geometry with these responses, we will focus solely on s-wave superconductors, since for d-wave superconductors, as observed in the previous chapter, their quantum metric exhibits singular behavior around the nodal points and their fidelity number diverges. Hence, considering the case of s-wave superconductors, we will make certain approximations to the coherence factors that will allow us to relate it to quantum geometry and subsequently express the electromagnetic responses analytically using a continuous model, which is explained in detail in appendix C, obtaining as a relevant result that these responses are related to quantum geometry through the quantum metric and the fidelity number.

4.1
Infrared absorption in singlet superconductors

In this section, we will calculate the infrared absorption in singlet superconductors, as we demonstrated in appendix B, the infrared absorption corresponds to the real part of the conductivity eq. (B-16), which can be expressed, after a Fourier transform of eq. (B-16), as follows

$$\mathrm{Re}\,\sigma(\mathbf{q},\omega) = \frac{1}{\omega}\mathrm{Im}\left[\pi(\mathbf{q},\omega)\right], \tag{4-1}$$

where $\pi(\mathbf{q},\omega)$ is the current-current correlator. Before proceeding with the corresponding calculations, we will define the conditions of the system.

Let's assume that we have a singlet superconductor, which is subjected to a transverse electromagnetic wave polarized in the direction $\hat{\boldsymbol{\mu}}$ and propagating in the direction $\hat{\boldsymbol{\nu}}$, with a small wave vector $\mathbf{q} = q\hat{\nu}$, in such a way that both are

perpendicular. In accordance with what was mentioned in appendix B.1, the perturbative Hamiltonian in D-dimensions due to this electromagnetic wave is expressed as

$$H' = -a^D j_\mu(\mathbf{q}) A_\mu(\mathbf{q}, t), \tag{4-2}$$

where $A_\mu(\mathbf{q}, t) = \sum_{\mathbf{r}} A_\mu(\mathbf{r}, t) e^{i\mathbf{q}\cdot\mathbf{r}}$ is the Fourier transform of the time-dependent vector field polarized along $\hat{\boldsymbol{\mu}}$. The term $j_\mu(\mathbf{q})$ represents the current density operator and is given by the following expression

$$j_\mu(\mathbf{q}) = \frac{e}{a^D} \sum_k v_\mu(\mathbf{k}) c^\dagger_{\mathbf{k}+\mathbf{q}\sigma} c_{\mathbf{k}\sigma}, \tag{4-3}$$

where the term $v_\mu(\mathbf{k}) = \partial_\mu \varepsilon_{\mathbf{k}}$ is the group velocity of the normal state at $\mathbf{k}$, with $\varepsilon_{\mathbf{k}}$ being the normal state dispersion. In order to calculate eq. (4-1), we proceed by defining the Matsubara current-current correlator as

$$\pi(\mathbf{q}, i\omega) = -\frac{a^D}{\hbar} \int_0^\beta d\tau \, e^{i\omega\tau} \langle T_\tau j_\mu(\mathbf{q}, \tau), j_\mu(-\mathbf{q}, 0) \rangle. \tag{4-4}$$

We can express $\pi(\mathbf{q}, i\omega)$ in terms of the polarization operator, defined in eq. (A-1), as follows

$$\pi(\mathbf{q}, i\omega) = \frac{e^2}{a^D} \sum_k v_\mu^2 P(\mathbf{k}, \mathbf{q}, i\omega). \tag{4-5}$$

Continuing with the application of the analytical continuation $\pi_{\mu\nu}(\mathbf{q}, \omega) = \pi_{\mu\nu}(\mathbf{q}, i\omega \to \hbar\omega + i\eta)$, we have

$$\pi(\mathbf{q}, \omega) = \frac{e^2}{a^D} \sum_k v_\mu^2 P(\mathbf{k}, \mathbf{q}, \omega). \tag{4-6}$$

Since we are considering the case of zero temperature, we can use the expression for the polarization operator $P_0(\mathbf{k}, \mathbf{q}, \omega)$, calculated in appendix A, given by eq. (A-13). We can now calculate the conductivity $\sigma_{\mu\mu}(\mathbf{q}, \omega) \equiv \sigma(\mathbf{q}, \omega)$ along the polarization direction $\hat{\mu}$. As we are interested in infrared absorption, we must calculate $\mathrm{Im}\,[\pi(\mathbf{q}, \omega)]$, for which we proceed to use eq. (4-6) considering only the imaginary part of $P_0(\mathbf{k}, \mathbf{q}, \omega)$, given by eq. (A-14). Subsequently, we replace $\mathrm{Im}\,[\pi(\mathbf{q}, \omega)]$ in eq. (4-1), obtaining after a momentum integration

$$\mathrm{Re}\,\sigma(\mathbf{q}, \omega) = \frac{2\pi e^2}{\omega} \int \frac{d^D\mathbf{k}}{(2\pi\hbar)^D} v_\mu^2 \left[u^2_{\mathbf{k}+\mathbf{q}} v^2_{\mathbf{k}} - u_{\mathbf{k}} v_{\mathbf{k}} u_{\mathbf{k}+\mathbf{q}} v_{\mathbf{k}+\mathbf{q}} \right] \delta(\hbar\omega - E_{\mathbf{k}} - E_{\mathbf{k}+\mathbf{q}}). \tag{4-7}$$

Thus, the expression above allows us to calculate infrared absorption. Finally, the expression eq. (4-7) contains a coherence factor given by the terms $u^2_{\mathbf{k}+\mathbf{q}} v^2_{\mathbf{k}} - u_{\mathbf{k}} v_{\mathbf{k}} u_{\mathbf{k}+\mathbf{q}} v_{\mathbf{k}+\mathbf{q}}$, which will be discussed later for s-wave superconductors.

4.2 Paramagnetic current in singlet superconductors

The London equation in the presence of a static field vector with wave vector $\mathbf{q} = q\hat{\nu}$ is expressed as follows [61]

$$J_\mu = J_{\mu 1} + J_{\mu 2}, \tag{4-8}$$

where it is expressed in the London gauge, and we also observe that it agrees with what is seen in appendix B.1. In eq. (4-8), the term $J_{\mu 2}$ represents the diamagnetic current, which is used in London's theory, as seen in section 2.2, and therefore is associated with the Meissner effect, and $J_{\mu 1}$ is the paramagnetic current, so named because it tends to cancel out the diamagnetic current $J_{\mu 2}$ [61]. We will focus on the calculation of the paramagnetic current in the presence of a static vector field. Linear response theory assumes that the system's response $J_{\mu 1}$ is proportional to the perturbation given by the static vector field, and the proportionality constant is given by K_1 as follows

$$J_{\mu 1} = -K_1(\mathbf{q})\mathbf{A}_\mu(\mathbf{q}), \tag{4-9}$$

where K_1 is the response coefficient associated with the paramagnetic current and $\mathbf{A}_\mu(\mathbf{q})$ is the Fourier component of the time-independent vector field polarized along $\hat{\boldsymbol{\mu}}$. Since this term is a static response, it relates to the real part of the Matsubara current-current correlator

$$K_1(\mathbf{q}) = \operatorname{Re}\pi(\mathbf{q}, 0)|_{T=0}. \tag{4-10}$$

Thus, to calculate $K_1(\mathbf{q})$, we have to use eq. (4-6) considering only the real part of the polarization operator and the limit $\omega = 0$

$$\operatorname{Re}\pi(\mathbf{q}, 0)|_{T=0} = \frac{e^2}{a^D}\sum_{\mathbf{k}} v_\mu^2 \operatorname{Re} P_0(\mathbf{k}, \mathbf{q}, 0). \tag{4-11}$$

Next, we replace eq. (A-15) into eq. (4-11), which leads us to obtain the coefficient response expressed as follows

$$K_1(\mathbf{q}) = -2e^2 \int \frac{d^D\mathbf{k}}{(2\pi\hbar)^D} v_\mu^2 \frac{\left(u_{\mathbf{k}+\mathbf{q}}v_{\mathbf{k}} - v_{\mathbf{k}+\mathbf{q}}u_{\mathbf{k}}\right)^2}{E_{\mathbf{k}} + E_{\mathbf{k}+\mathbf{q}}}. \tag{4-12}$$

We observe that this last expression contains the following coherence factor $\left(u_{\mathbf{k}+\mathbf{q}}v_{\mathbf{k}} - v_{\mathbf{k}+\mathbf{q}}u_{\mathbf{k}}\right)^2$, which as we will show later is related to the quantum metric for s-wave superconductors.

4.3 Linear screening in singlet superconductors

We are interested in studying screening for the case of $\omega = 0$ in singlet superconductors. Then, we will calculate the static dielectric function $\varepsilon(\mathbf{q}, 0)$. Considering what is shown in appendix B and the definition given for the polarization operator in eq. (A-1), we can express the static dielectric function as follows

$$\varepsilon(\mathbf{q}, 0) = 1 - V_{\mathbf{q}} P_0(\mathbf{q}, 0), \tag{4-13}$$

where $V(\mathbf{q}) = \sum_{\mathbf{r}} e^{i\mathbf{q}\cdot\mathbf{r}} V(\mathbf{r})$ is the Fourier transform of the Coulomb potential. On the other hand, the term $P_0(\mathbf{q}, 0)$ is defined as follows

$$P_0(\mathbf{q}, 0) = \int \frac{d^D\mathbf{k}}{(2\pi\hbar/a)^D} \operatorname{Re} P_0(\mathbf{k}, \mathbf{q}, 0), \tag{4-14}$$

where we observe the term $\operatorname{Re} P_0(\mathbf{k}, \mathbf{q}, 0)$, which we have calculated in appendix A. So, by replacing eq. (A-14) into eq. (4-14), we obtain

$$P_0(\mathbf{q}, 0) = -2 \int \frac{d^D\mathbf{k}}{(2\pi\hbar/a)^D} \frac{\left(u_{\mathbf{k}+\mathbf{q}} v_{\mathbf{k}} - v_{\mathbf{k}+\mathbf{q}} u_{\mathbf{k}}\right)^2}{E_{\mathbf{k}} + E_{\mathbf{k}+\mathbf{q}}}. \tag{4-15}$$

We can verify that the expression above has the same coherence factor as in the case of the paramagnetic current, hence we will later show how $P_0(\mathbf{q}, 0)$ is related to the quantum metric for s-wave superconductors.

4.4 Electromagnetic responses in s-wave superconductors

As previously analyzed, electromagnetic responses such as infrared absorption, the paramagnetic current, and the dielectric function are related to coherence factors. We will now focus on the relationship between these coherence factors and the quantum metric for the case of s-wave superconductors, considering some approximations that will be detailed below.

Approximation of coherence factors

In s-wave superconductors, the superconducting gap is of the order $\Delta \sim 0.01$ eV, so the minimum wave vector of light that can excite quasiparticles is much smaller than the Fermi momentum $q \ll k_F$. This allows us to expand the coherence factors in terms of q to the first or second order as we will do below.

For the case of infrared absorption, we will expand the coherence factor up to second order in $\mathbf{q} = q\hat{\nu}$, which we obtain in eq. (4-7), obtaining

$$\begin{aligned} u^2_{\mathbf{k}+\mathbf{q}} v^2_{\mathbf{k}} - u_{\mathbf{k}} v_{\mathbf{k}} u_{\mathbf{k}+\mathbf{q}} v_{\mathbf{k}+\mathbf{q}} &\approx (q u_{\mathbf{k}} v_{\mathbf{k}} + q^2 v_k \partial_\nu u_{\mathbf{k}})(v_{\mathbf{k}} \partial_\nu u_{\mathbf{k}} - u_{\mathbf{k}} \partial_\nu v_{\mathbf{k}}) \\ &= \left(\frac{q\Delta}{2E_{\mathbf{k}}} + \frac{q^2 \Delta^3 v_\nu}{4(E_{\mathbf{k}} + \varepsilon_{\mathbf{k}}) E^3_{\mathbf{k}}} \right) \frac{\Delta v_\nu}{2E^2_{\mathbf{k}}}. \end{aligned} \tag{4-16}$$

On the other hand, in the case of the paramagnetic current and the dielectric function, we will expand the coherence factor that appears in both eqs. (4-12) and (4-15), obtaining

$$(u_{\mathbf{k}+\mathbf{q}} v_{\mathbf{k}} - v_{\mathbf{k}+\mathbf{q}} u_{\mathbf{k}})^2 \approx q^2 (v_{\mathbf{k}} \partial_\nu u_{\mathbf{k}} - u_{\mathbf{k}} \partial_\nu v_{\mathbf{k}}) = q^2 g_{\nu\nu}, \tag{4-17}$$

where we observe the appearance of the diagonal element of the quantum metric $g_{\nu\nu}$ along $\mathbf{q}$. We proceed to use these approximations given by eqs. (4-16) and (4-17) to calculate the electromagnetic responses for s-wave superconductors.

Infrared absorption in s-wave superconductors

For infrared absorption in 3D, we will use eq. (4-7) in which we will replace eq. (4-16) and, due to the argument made in section 4.4, we can use the following approximation for the argument of the δ-function $\hbar\omega - E_{\mathbf{k}} - E_{\mathbf{k}+\mathbf{q}} \approx \hbar\omega - 2E_{\mathbf{k}}$. Additionally, as we saw, eq. (4-16) is composed of a first-order term and another in second order in $\mathbf{q} = q\hat{\nu}$, so for the first order we have

$$\mathrm{Re}\,\sigma^{1st}(\mathbf{q},\omega) \approx \pi e^2 \hbar q \int \frac{d^3\mathbf{k}}{(2\pi\hbar)^3} g_{\mu\mu} v_\nu \delta(\hbar\omega - 2E_{\mathbf{k}}), \tag{4-18}$$

resulting in zero due to the even parity of the metric $g_{\mu\mu}$ and the odd parity of the normal state group velocity v_ν. On the other hand, for the second-order term, we have

$$\mathrm{Re}\,\sigma^{2nd}(\mathbf{q},\omega) \approx 2\pi e^2 \frac{\hbar q^2}{2m} \int \frac{d^3\mathbf{k}}{(2\pi\hbar)^3} \left[\frac{m v_\nu^2 \Delta^2}{E_{\mathbf{k}}^2 (E_{\mathbf{k}} + \varepsilon_{\mathbf{k}})}\right] g_{\mu\mu} \delta(\hbar\omega - 2E_{\mathbf{k}}). \tag{4-19}$$

Thus, we see that the quantum metric appears in the integrand of this second order term, but with an extra factor that depends on the energy, gap, and velocity due to the Bogoluibov transformation. For the 2D case, we need to reduce the dimension of the integral from eq. (4-19) in the following manner $\int d^3\mathbf{k}/(2\pi\hbar)^3 \rightarrow \int d^2\mathbf{k}/(2\pi\hbar)^2$, where it can be observed that the quantum metric appears in the integrand along with other parameters as in the 3D case.

Paramagnetic current in s-wave superconductors

For the paramagnetic current, we need to calculate the response coefficient K_1 given by eq. (4-12) where we will replace eq. (4-17) and use the following approximation $E_{\mathbf{k}} + E_{\mathbf{k}+\mathbf{q}} \approx 2E_{\mathbf{k}}$, resulting in

$$K_1^{3D}(\mathbf{q}) \approx -e^2 q^2 \int \frac{d^3\mathbf{k}}{(2\pi\hbar)^3} v_\mu^2 \frac{g_{\nu\nu}}{E_{\mathbf{k}}}, \tag{4-20}$$

where the analytical expression of this equation, which is calculated in appendix C, is given by the following equation

$$K_1^{3D}(\mathbf{q}) = -e^2 \frac{4\pi^6 f(\alpha)}{\sqrt{10} m a^3} \left(\frac{\xi}{a}\right)^2 \left(\frac{q}{2\pi\hbar/a}\right)^2 \left(\frac{k_F}{2\pi\hbar/a}\right)^3, \tag{4-21}$$
$$f(\alpha) \equiv \frac{4}{15} + \frac{2}{15}\cos^2\alpha,$$

where α is the angle between the propagation direction $\hat{\boldsymbol{\mu}}$ and the polarization $\hat{\boldsymbol{\nu}}$. The factor $[k_F/(2\pi\hbar/a)]^3$ can be considered as the volume of the Fermi sea measured in units of the Brillouin zone, $q/(2\pi\hbar/a)$ is the spatial modulation of the vector field measured in units of Fermi momentum, and e^2/ma^3 provides the correct units.

Using eq. (3-37) in eq. (4-21), we can arrive at the following expression

$$K_1^{3D}(\mathbf{q}) = -\frac{288\pi^2}{\sqrt{10}} \frac{f(\alpha) e^2}{m a^3} \left(\frac{q}{2\pi\hbar/a}\right)^2 \left(\frac{k_F}{2\pi\hbar/a}\right)^{-1} \left(\frac{\mathcal{G}_{\nu\nu}^{3D}}{\hbar/a}\right)^2. \tag{4-22}$$

This implies that the coefficient $K_1^{3D}(\mathbf{q})$ is determined by the coherence length, which is synonymous with the fidelity number. We also observe that it has a quadratic dependence on q, which has been previously found in the literature [61]. On the other hand, when calculating the expression for $K_1(\mathbf{q})$ in the 2D case, as seen in appendix C.2, we have

$$K_1^{2D}(\mathbf{q}) = -\frac{2\pi^5 e^2 \overline{f}(\alpha)}{\sqrt{10} m a^2} \left(\frac{q}{2\pi\hbar/a}\right)^2 \left(\frac{\xi}{a}\right)^2 \left(\frac{k_F}{2\pi\hbar/a}\right)^2, \tag{4-23}$$

$$K_1^{2D}(\mathbf{q}) = -\frac{2\pi^5 e^2 \overline{f}(\alpha)}{\sqrt{10} m a^2} \left(\frac{q}{2\pi\hbar/a}\right)^2 (\mathcal{G}_{\nu\nu}^{2D})^2, \tag{4-24}$$

$$\overline{f}(\alpha) \equiv \frac{\pi}{4} + \frac{\pi}{2}\cos^2\alpha.$$

It is observed, as for the 3D case, that the response coefficient is proportional to the square of the fidelity number, indicating the relationship that exists between the paramagnetic current and the quantum geometry for 3D and 2D.

Dielectric function in s-wave superconductors

For this electromagnetic response, we need to calculate $P_0(\mathbf{q}, 0)$ given by eq. (4-15), this is done by replacing eq. (4-17) and using again the approximation $E_{\mathbf{k}} + E_{\mathbf{k}+\mathbf{q}} \approx 2E_{\mathbf{k}}$, obtaining

$$P_0^{3D}(\mathbf{q}, 0) \approx q^2 \int \frac{d^3\mathbf{k}}{(2\pi\hbar/a)^3} \frac{g_{\nu\nu}}{E_{\mathbf{k}}}. \tag{4-25}$$

The analytical formulation of eq. (4-25), detailed in appendix C, is

$$P_0^{3D}(\mathbf{q},0) = -\frac{4\pi^4}{3\sqrt{10}\Delta}\left(\frac{\xi}{a}\right)\left(\frac{k_F}{2\pi\hbar/a}\right)^2\left(\frac{q}{2\pi\hbar/a}\right)^2, \tag{4-26}$$

$$P_0^{3D}(\mathbf{q},0) = -\frac{8\pi^2}{\sqrt{5}\Delta}\left(\frac{q}{2\pi\hbar/a}\right)^2\frac{\mathcal{G}_{\nu\nu}^{3D}}{\hbar/a}, \tag{4-27}$$

where we have used eq. (3-37) to express it in terms of the 3D fidelity number. So, we see that the linear screening is also determined by the coherence length and hence the fidelity number, signifying the influence of quantum geometry in the linear screening. On the other hand, for the 2D case, as seen in appendix C.2, we have the following expressions

$$P_0^{2D}(\mathbf{q},0) = -\frac{\pi^4}{\sqrt{10}\Delta}\left(\frac{\xi}{a}\right)\left(\frac{k_F}{2\pi\hbar/a}\right)\left(\frac{q}{2\pi\hbar/a}\right)^2,$$

$$P_0^{2D}(\mathbf{q},0) = -\frac{8\pi^2}{\sqrt{5}\Delta}\left(\frac{q}{2\pi\hbar/a}\right)^2\mathcal{G}_{\nu\nu}^{2D}, \tag{4-28}$$

which equivalently indicates, as in the 3D case, that $P_0^{2D}(\mathbf{q},0)$ is directly related to the fidelity number, showing that the static dielectric function is related to quantum geometry.

5
Conclusions

Throughout this work, we have presented a study of the quantum geometric properties of singlet superconductors such as s-wave and d-wave superconductors and their relationships with different electromagnetic properties: infrared absorption, the paramagnetic current, and the dielectric function. For the case of geometric properties, we studied the quantum metric, whose definition arises from the overlap of two quasihole states $|n\rangle$ defined at $\mathbf{k}$ and $\mathbf{k}+\delta\mathbf{k}$, which turns out to be non-trivial as it is different from zero. For s-wave superconductors, we showed how the quantum metric represents the twisting of the unit vector $\mathbf{w_k} = (v_\mathbf{k}, -u_\mathbf{k})$, formed with the Bogoliubov coefficients, in the Hilbert space. While for d-wave superconductors, we showed that the quantum metric diverges near their nodal points, which is represented by a dramatic twisting of the vector $\mathbf{w_k}$ forming vortices around these points.

We also studied the fidelity number, which is defined as the integral of the quantum metric over the Brillouin zone, and physically represents the average distance between two neighboring quasihole states. An important result we obtained is that for s-wave superconductors, the fidelity number is directly related to the coherence length, leading to the conclusion that if a property is related to the coherence length, then it must also be related to the fidelity number. On the other hand, for d-wave superconductors, we showed that since the quantum metric diverges near the nodal points, their fidelity number also diverges. Another quantity we studied is the fidelity marker, which represents the mapping at each lattice site of the fidelity number. We observed that for s-wave superconductors, introducing a nonmagnetic impurity locally suppresses the fidelity marker. Physically, this indicates that this impurity reduces the average distance between quasihole states in momentum space. Concluding that disorder modify the quantum geometric properties of s-wave superconductors.

Moreover, we explored electromagnetic responses such as infrared absorption, the paramagnetic current, and the dielectric function for singlet superconductors. Especially for s-wave superconductors, each of these responses was expressed in terms of the quantum metric or the fidelity number, thus showing that these responses are related to quantum geometry. On the other

hand, in the case of d-wave superconductors, we have not directly related the electromagnetic responses to the quantum geometry due to the singular behavior of the quantum metric around the nodal points, showing a divergent fidelity number.

Based on the foregoing, we can conclude that our work provides a detailed explanation of the quantum geometric properties of singlet superconductors and how these properties are susceptible to disorder. Furthermore, we demonstrate that they can be experimentally measured by making use of their relationship with electromagnetic responses. Future research based on our work could consider both the expansion of the results obtained for the case of non-zero temperature, as well as the exploration of other types of superconductors with different pairing symmetries, such as those of triplet superconductors.

Bibliography

[1] PROVOST, J.; VALLEE, G.. **Riemannian structure on manifolds of quantum states**. Communications in Mathematical Physics, 76:289–301, 1980.

[2] YANG, L.; MA, Y.-Q. ; LI, X.-G.. **Geometric tensor and the topological characterization of the bloch band in a two-band lattice model**. Physica B: Condensed Matter, 456:359–364, 2015.

[3] MA, Y.-Q.. **Quantum distance and the euler number index of the bloch band in a one-dimensional spin model**. Phys. Rev. E, 90:042133, Oct 2014.

[4] PALUMBO, G.. **Momentum-space cigar geometry in topological phases**. The European Physical Journal Plus, 133:1–8, 2018.

[5] XIAO, D.; CHANG, M.-C. ; NIU, Q.. **Berry phase effects on electronic properties**. Rev. Mod. Phys., 82:1959–2007, Jul 2010.

[6] NAGAOSA, N.; SINOVA, J.; ONODA, S.; MACDONALD, A. H. ; ONG, N. P.. **Anomalous hall effect**. Rev. Mod. Phys., 82:1539–1592, May 2010.

[7] VANDERBILT, D.. **Berry phases in electronic structure theory: electric polarization, orbital magnetization and topological insulators**. Cambridge University Press, 2018.

[8] BERNEVIG, B. A.. **Topological insulators and topological superconductors**. Princeton university press, 2013.

[9] OZAWA, T.; GOLDMAN, N.. **Extracting the quantum metric tensor through periodic driving**. Phys. Rev. B, 97:201117, May 2018.

[10] YU, M.; YANG, P.; GONG, M.; CAO, Q.; LU, Q.; LIU, H.; ZHANG, S.; PLENIO, M. B.; JELEZKO, F.; OZAWA, T.; GOLDMAN, N. ; CAI, J.. **Experimental measurement of the quantum geometric tensor using coupled qubits in diamond**. National Science Review, 7(2):254–260, 11 2019.

[11] TAN, X.; ZHANG, D.-W.; YANG, Z.; CHU, J.; ZHU, Y.-Q.; LI, D.; YANG, X.; SONG, S.; HAN, Z.; LI, Z.; DONG, Y.; YU, H.-F.; YAN, H.; ZHU, S.-L. ; YU, Y.. **Experimental measurement of the quantum metric tensor and related topological phase transition with a superconducting qubit**. Phys. Rev. Lett., 122:210401, May 2019.

[12] GIANFRATE, A.; BLEU, O.; DOMINICI, L.; ARDIZZONE, V.; DE GIORGI, M.; BALLARINI, D.; LERARIO, G.; WEST, K.; PFEIFFER, L.; SOLNYSHKOV, D. ; OTHERS. **Measurement of the quantum geometric tensor and of the anomalous hall drift**. Nature, 578(7795):381–385, 2020.

[13] CHEN, W.; VON GERSDORFF, G.. **Measurement of interaction-dressed Berry curvature and quantum metric in solids by optical absorption**. SciPost Phys. Core, 5:040, 2022.

[14] DE SOUSA, M. S. M.; CHEN, W.. **Opacity of graphene independent of light frequency and polarization due to the topological charge of the dirac points**. Phys. Rev. B, 108:165201, Oct 2023.

[15] DE SOUSA, M. S. M.; CRUZ, A. L. ; CHEN, W.. **Mapping quantum geometry and quantum phase transitions to real space by a fidelity marker**. Phys. Rev. B, 107:205133, May 2023.

[16] VON GERSDORFF, G.; CHEN, W.. **Measurement of topological order based on metric-curvature correspondence**. Phys. Rev. B, 104:195133, Nov 2021.

[17] SCHNYDER, A. P.; RYU, S.; FURUSAKI, A. ; LUDWIG, A. W. W.. **Classification of topological insulators and superconductors in three spatial dimensions**. Phys. Rev. B, 78:195125, Nov 2008.

[18] RYU, S.; SCHNYDER, A. P.; FURUSAKI, A. ; LUDWIG, A. W. W.. **Topological insulators and superconductors: tenfold way and dimensional hierarchy**. New Journal of Physics, 12(6):065010, jun 2010.

[19] KITAEV, A.. **Periodic table for topological insulators and superconductors**. AIP Conference Proceedings, 1134(1):22–30, 05 2009.

[20] CHIU, C.-K.; TEO, J. C. Y.; SCHNYDER, A. P. ; RYU, S.. **Classification of topological quantum matter with symmetries**. Rev. Mod. Phys., 88:035005, Aug 2016.

[21] PIÉCHON, F.; RAOUX, A.; FUCHS, J.-N. ; MONTAMBAUX, G.. **Geometric orbital susceptibility: Quantum metric without berry curvature**. Phys. Rev. B, 94:134423, Oct 2016.

[22] MA, Y.-Q.. **Euler characteristic number of the energy band and the reason for its non-integer values**, 2020.

[23] PALUMBO, G.; GOLDMAN, N.. **Revealing tensor monopoles through quantum-metric measurements**. Phys. Rev. Lett., 121:170401, Oct 2018.

[24] SALERNO, G.; GOLDMAN, N. ; PALUMBO, G.. **Floquet-engineering of nodal rings and nodal spheres and their characterization using the quantum metric**. Phys. Rev. Res., 2:013224, Feb 2020.

[25] PEOTTA, S.; TÖRMÄ, P.. **Superfluidity in topologically nontrivial flat bands**. Nature Communications, 6(1):8944, Nov 2015.

[26] JULKU, A.; PEOTTA, S.; VANHALA, T. I.; KIM, D.-H. ; TÖRMÄ, P.. **Geometric origin of superfluidity in the lieb-lattice flat band**. Phys. Rev. Lett., 117:045303, Jul 2016.

[27] LIANG, L.; VANHALA, T. I.; PEOTTA, S.; SIRO, T.; HARJU, A. ; TÖRMÄ, P.. **Band geometry, berry curvature, and superfluid weight**. Phys. Rev. B, 95:024515, Jan 2017.

[28] CAO, Y.; FATEMI, V.; FANG, S.; WATANABE, K.; TANIGUCHI, T.; KAXIRAS, E. ; JARILLO-HERRERO, P.. **Unconventional superconductivity in magic-angle graphene superlattices**. Nature, 556(7699):43–50, 2018.

[29] YANKOWITZ, M.; CHEN, S.; POLSHYN, H.; ZHANG, Y.; WATANABE, K.; TANIGUCHI, T.; GRAF, D.; YOUNG, A. F. ; DEAN, C. R.. **Tuning superconductivity in twisted bilayer graphene**. Science, 363(6431):1059–1064, 2019.

[30] HERZOG-ARBEITMAN, J.; PERI, V.; SCHINDLER, F.; HUBER, S. D. ; BERNEVIG, B. A.. **Superfluid weight bounds from symmetry and quantum geometry in flat bands**. Phys. Rev. Lett., 128:087002, Feb 2022.

[31] TÖRMÄ, P.; PEOTTA, S. ; BERNEVIG, B. A.. **Superconductivity, superfluidity and quantum geometry in twisted multilayer systems**. Nature Reviews Physics, 4(8):528–542, 2022.

[32] ISKIN, M.. **Extracting quantum-geometric effects from ginzburg-landau theory in a multiband hubbard model**. Phys. Rev. B, 107:224505, Jun 2023.

[33] GAVROGLU, K.. **On some myths regarding the liquefaction of hydrogen and helium**. European Journal of Physics, 15(1):9–15, Jan. 1994.

[34] ONNES, H. K.. **Through Measurement to Knowledge**. Springer Netherlands, 1990.

[35] SMITH, H. G.; WILHELM, J. O.. **Superconductivity**. Rev. Mod. Phys., 7:237–271, Oct 1935.

[36] FORREST, A. M.. **Meissner and ochsenfeld revisited**. European Journal of Physics, 4(2):117–120, Apr. 1983.

[37] LONDON, F.; LONDON, H.. **The electromagnetic equations of the supraconductor**. Proceedings of the Royal Society of London. Series A - Mathematical and Physical Sciences, 149(866):71–88, Mar. 1935.

[38] GINZBURG, V. L.. **On the theory of superconductivity**. Il Nuovo Cimento (1955-1965), 2:1234–1250, 1955.

[39] GINZBURG, V. L.; GINZBURG, V. L. ; LANDAU, L.. **On the theory of superconductivity**. Springer, 2009.

[40] REYNOLDS, C. A.; SERIN, B.; WRIGHT, W. H. ; NESBITT, L. B.. **Superconductivity of isotopes of mercury**. Physical Review, 78(4):487–487, May 1950.

[41] MAXWELL, E.. **Isotope effect in the superconductivity of mercury**. Physical Review, 78(4):477–477, May 1950.

[42] BARDEEN, J.; COOPER, L. N. ; SCHRIEFFER, J. R.. **Theory of superconductivity**. Phys. Rev., 108:1175–1204, Dec 1957.

[43] COOPER, L. N.. **Bound electron pairs in a degenerate fermi gas**. Phys. Rev., 104:1189–1190, Nov 1956.

[44] BRUUS, H.; FLENSBERG, K.. **Many-body quantum theory in condensed matter physics: an introduction**. OUP Oxford, 2004.

[45] COMBESCOT, R.. **Superconductivity: An Introduction**. Cambridge University Press, Mar. 2022.

[46] POOLE, C. P.; FARACH, H. A.; CRESWICK, R. J. ; PROZOROV, R.. **Superconductivity**. Elsevier, 2014.

[47] ABD-SHUKOR, R.. **Coherence length versus transition temperature of hydride-based and room temperature superconductors**. Results in Physics, 25:104219, June 2021.

[48] MAKI, K.. **Introduction to d-wave superconductivity**. In: AIP CONFERENCE PROCEEDINGS. American Institute of Physics, 1998.

[49] XIANG, T.; WU, C.. **D-wave Superconductivity**. Cambridge University Press, 2022.

[50] KOLODRUBETZ, M.; GRITSEV, V. ; POLKOVNIKOV, A.. **Classifying and measuring geometry of a quantum ground state manifold**. Phys. Rev. B, 88:064304, Aug 2013.

[51] KOLODRUBETZ, M.; SELS, D.; MEHTA, P. ; POLKOVNIKOV, A.. **Geometry and non-adiabatic response in quantum and classical systems**. Physics Reports, 697:1–87, 2017. Geometry and non-adiabatic response in quantum and classical systems.

[52] MA, Y.-Q.; GU, S.-J.; CHEN, S.; FAN, H. ; LIU, W.-M.. **The euler number of bloch states manifold and the quantum phases in gapped fermionic systems**. Europhysics Letters, 103(1):10008, jul 2013.

[53] MATSUURA, S.; RYU, S.. **Momentum space metric, nonlocal operator, and topological insulators**. Phys. Rev. B, 82:245113, Dec 2010.

[54] MARZARI, N.; VANDERBILT, D.. **Maximally localized generalized wannier functions for composite energy bands**. Phys. Rev. B, 56:12847–12865, Nov 1997.

[55] MARZARI, N.; MOSTOFI, A. A.; YATES, J. R.; SOUZA, I. ; VANDERBILT, D.. **Maximally localized wannier functions: Theory and applications**. Rev. Mod. Phys., 84:1419–1475, Oct 2012.

[56] ASHCROFT, N. W.; MERMIN, N. D.. **Solid state physics**. Cengage Learning, 2022.

[57] PORLLES, D.; CHEN, W.. **Quantum geometry of singlet superconductors**. Physical Review B, 108(9), Sept. 2023.

[58] DAMASCELLI, A.; HUSSAIN, Z. ; SHEN, Z.-X.. **Angle-resolved photoemission studies of the cuprate superconductors**. Rev. Mod. Phys., 75:473–541, Apr 2003.

[59] KEIMER, B.; KIVELSON, S. A.; NORMAN, M. R.; UCHIDA, S. ; ZAANEN, J.. **From quantum matter to high-temperature superconductivity in copper oxides**. Nature, 518(7538):179–186, Feb 2015.

[60] NUNNER, T. S.; CHEN, W.; ANDERSEN, B. M.; MELIKYAN, A. ; HIRSCHFELD, P. J.. **Fourier transform spectroscopy of d-wave quasiparticles in the presence of atomic scale pairing disorder**. Phys. Rev. B, 73:104511, Mar 2006.

[61] TINKHAM, M.. **Introduction to Superconductivity, volume Second Edition**. Dover Publications Inc., Mineola, New York, 2004.

[62] MAHAN, G. D.. **Many-particle physics**. Springer Science & Business Media, 2000.

[63] COLEMAN, P.. **Introduction to many-body physics**. Cambridge University Press, 2015.

[64] GIULIANI, G.; VIGNALE, G.. **Quantum Theory of the Electron Liquid**. Cambridge University Press, Mar. 2005.

A
Polarization operator is singlet superconductors

The electromagnetic responses are linked to different response functions. For instance, in the appendix B, we will see that conductivity is associated with the current-current correlator, and the dielectric function is related to the density-density correlator. Both response functions are, in turn, related to the polarization operator [62]. Due to this connection with the polarization operator, the present appendix will focus on characterizing this operator for singlet superconductors. This approach is adopted with the aim of using such characterization to express the specific response functions for this type of superconductors.

We will begin by defining the polarization operator in general terms using the Matsubara formalism [62] as

$$P(\mathbf{k},\mathbf{q},i\omega) = -\frac{1}{\hbar}\sum_{\sigma\sigma'}\int_0^\beta d\tau e^{i\omega\tau}\langle T_\tau c^\dagger_{\mathbf{k}+\mathbf{q}\sigma}(\tau)c_{\mathbf{k}\sigma}(\tau)c^\dagger_{\mathbf{k}'-\mathbf{q}\sigma'}(0)c_{\mathbf{k}'\sigma'}(0)\rangle. \quad \text{(A-1)}$$

Now we proceed to apply Wick's theorem. This theorem states that the ensemble average of a series of operators can be decomposed into the sum of all their possible contractions, where a contraction is the ensemble average of a pair of operators. Thus, by applying this theorem to the term $\langle ...\rangle$ in eq. (A-1), and considering only those contractions that are nonzero, we have

$$\begin{aligned}\langle ...\rangle = &\langle T_\tau c^\dagger_{\mathbf{k}+\mathbf{q}\sigma}(\tau)c_{\mathbf{k}\sigma}(\tau)\rangle\langle T_\tau c^\dagger_{\mathbf{k}'-\mathbf{q}\sigma}(0)c_{\mathbf{k}'\sigma'}(0)\rangle \\ &+ \langle T_\tau c^\dagger_{\mathbf{k}+\mathbf{q}\sigma}(\tau)c^\dagger_{\mathbf{k}'-\mathbf{q}\sigma'}(\tau)\rangle\langle T_\tau c_{\mathbf{k}\sigma}(\tau)c_{\mathbf{k}'\sigma'}(\tau)\rangle \\ &+ \langle T_\tau c^\dagger_{\mathbf{k}+\mathbf{q}\sigma}(\tau)c_{\mathbf{k}'\sigma'}(0)\rangle\langle T_\tau c_{\mathbf{k}\sigma}(\tau)c^\dagger_{\mathbf{k}'-\mathbf{q}\sigma'}(0)\rangle.\end{aligned} \quad \text{(A-2)}$$

We proceed by substituting eq. (A-2) into eq. (A-1) and applying the summation, we obtain

$$P(\mathbf{k},\mathbf{q},i\omega) = -\frac{1}{\hbar}\int_0^\beta d\tau e^{i\omega\tau}[G(\mathbf{k},\tau)G(\mathbf{k}+\mathbf{q},-\tau) + F(\mathbf{k},\tau)F^\dagger(\mathbf{k}+\mathbf{q},-\tau)], \quad \text{(A-3)}$$

where $G(\mathbf{k},\tau)$ and $F(\mathbf{k},\tau)$ are the Green's functions used to address the BCS theory [44, 62]. We can also express eq. (A-3) in the following way

$$P(\mathbf{k},\mathbf{q},i\omega) = \frac{2}{\beta}\sum_{ip}[G(\mathbf{k},ip)G(\mathbf{k}+\mathbf{q},ip+i\omega)+F(\mathbf{k},ip)F^\dagger(\mathbf{k}+\mathbf{q},ip+i\omega)], \quad \text{(A-4)}$$

where $i\omega$ and ip are Matsubara frequencies. We can also express the Green's functions in terms of the Bogoliubov coefficients as follows [62]

$$G(\mathbf{k}, ip) = \frac{u_{\mathbf{k}}^2}{ip - E_{\mathbf{k}}} + \frac{v_{\mathbf{k}}^2}{ip + E_{\mathbf{k}}}, \tag{A-5}$$

$$F(\mathbf{k}, ip) = F^{\dagger}(\mathbf{k}, ip) = -u_{\mathbf{k}} v_{\mathbf{k}} \left(\frac{1}{ip - E_{\mathbf{k}}} + \frac{1}{ip + E_{\mathbf{k}}} \right). \tag{A-6}$$

Next, we use the frequency summations [62] which allow us to obtain the following expressions

$$\frac{1}{\beta} \sum_{ip} \frac{1}{ip - E_{\mathbf{k}}} \frac{1}{ip + i\omega - E_{\mathbf{k+q}}} = \frac{n_{\mathbf{k}} - n_{\mathbf{k+q}}}{i\omega + E_{\mathbf{k}} - E_{\mathbf{k+q}}}, \tag{A-7}$$

$$-\frac{1}{\beta} \sum_{ip} \frac{1}{ip - E_{\mathbf{k}}} \frac{1}{i\omega - ip - E_{\mathbf{k+q}}} = \frac{1 - n_{\mathbf{k}} - n_{\mathbf{k+q}}}{i\omega - E_{\mathbf{k}} - E_{\mathbf{k+q}}}. \tag{A-8}$$

So, using these eqs. (A-7) and (A-8), we can arrive at the following results

$$\begin{aligned} \frac{2}{\beta} \sum_{ip} G(\mathbf{k}, ip) G(\mathbf{k} + \mathbf{q}, ip + i\omega) = \\ [1 - n_k - n_{k+q}] \left(\frac{v_k^2 u_{k+q}^2}{i\omega - E_k - E_{k+q}} - \frac{u_k^2 v_{k+q}^2}{i\omega - E_k - E_{k+q}} \right) \\ + [n_k - n_{k+q}] \left(\frac{u_k^2 u_{k+q}^2}{i\omega + E_k - E_{k+q}} - \frac{v_k^2 v_{k+q}^2}{i\omega - E_k + E_{k+q}} \right), \end{aligned} \tag{A-9}$$

and

$$\begin{aligned} \frac{2}{\beta} \sum_{ip} F(\mathbf{k}, ip) F^{\dagger}(\mathbf{k} + \mathbf{q}, ip + i\omega) = u_k v_k u_{k+q} v_{k+q} \Bigg[& \frac{1}{i\omega + E_k - E_{k+q}} (n_k - n_{k+q}) \\ & + \frac{1}{i\omega + E_k + E_{k+q}} (1 - n_k - n_{k+q}) \\ & - \frac{1}{i\omega - E_k - E_{k+q}} (1 - n_k - n_{k+q}) \\ & - \frac{1}{i\omega - E_k + E_{k+q}} (n_k - n_{k+q}) \Bigg]. \end{aligned} \tag{A-10}$$

Considering the case where we are at zero temperature, there would be no quasiparticles so $n_{\mathbf{k}} = n_{\mathbf{k+q}} = 0$, and eqs. (A-9) and (A-10) would reduce to

$$\frac{2}{\beta} \sum_{ip} G(\mathbf{k}, ip) G(\mathbf{k} + \mathbf{q}, ip + i\omega) = \frac{v_k^2 u_{k+q}^2}{i\omega - E_k - E_{k+q}} - \frac{u_k^2 v_{k+q}^2}{i\omega - E_k - E_{k+q}}, \tag{A-11}$$

and

$$\frac{2}{\beta}\sum_{ip} F(\mathbf{k},ip)F^{\dagger}(\mathbf{k}+\mathbf{q},ip+i\omega) = u_{\mathbf{k}}v_{\mathbf{k}}u_{\mathbf{k+q}}v_{\mathbf{k+q}}\times \left[\frac{1}{i\omega+E_{\mathbf{k}}+E_{\mathbf{k+q}}}-\frac{1}{i\omega-E_{\mathbf{k}}-E_{\mathbf{k+q}}}\right]. \tag{A-12}$$

We then proceed to substitute eqs. (A-11) and (A-12) into eq. (A-4), and after applying the analytical continuation $i\omega \to \hbar\omega + i\eta$, where η is a small artificial broadening, we can express the polarization operator at zero temperature for s-wave superconductors as follows

$$P_0(\mathbf{k},\mathbf{q},\omega) = 2\left[\frac{u^2_{\mathbf{k+q}}v^2_{\mathbf{k}}-u_{\mathbf{k}}v_{\mathbf{k}}u_{\mathbf{k+q}}v_{\mathbf{k+q}}}{\hbar\omega-E_{\mathbf{k}}-E_{\mathbf{k+q}}+i\eta}-\frac{v^2_{\mathbf{k+q}}u^2_{\mathbf{k}}-u_{\mathbf{k}}v_{\mathbf{k}}u_{\mathbf{k+q}}v_{\mathbf{k+q}}}{\hbar\omega+E_{\mathbf{k}}+E_{\mathbf{k+q}}+i\eta}\right]. \tag{A-13}$$

The expression above represents the polarization operator for a singlet superconductor at zero temperature. The expression in eq. (A-13) allows us to study both dissipative and non-dissipative processes.

Dissipative processes correspond to dynamic responses of the system, such as emission and absorption processes that are related to the imaginary part of the polarization operator. Meanwhile, the real part of this operator is linked to non-dissipative processes, which provide information about the static responses of the system, for example, when considering electromagnetic perturbations with frequencies $\omega = 0$.

In this dissertation, we will focus on the study of two types of situations. On one hand, the optical absorption process, which will allow us to study infrared absorption in s-wave superconductors and corresponds to the excitation of quasiparticles. This process corresponds to the imaginary part of the first term of eq. (A-13) at a finite frequency, obtaining

$$-\frac{1}{\pi}\mathrm{Im}P_o(\mathbf{k},\mathbf{q},\omega) = 2\left[u^2_{\mathbf{k+q}}v^2_{\mathbf{k}}-u_{\mathbf{k}}v_{\mathbf{k}}u_{\mathbf{k+q}}v_{\mathbf{k+q}}\right]\delta(\hbar\omega-E_{\mathbf{k}}-E_{\mathbf{k+q}}), \tag{A-14}$$

where the delta function ensures the conservation of energy and momentum. On the other hand, we will also study static responses of the system, such as the paramagnetic current and the dielectric function, both for $\omega = 0$. These responses are related to the real part of both terms of eq. (A-13) in the $\omega = 0$ limit, which gives us

$$\mathrm{Re}P_0(\mathbf{k},\mathbf{q},0) = \frac{2\left(u_{\mathbf{k+q}}v_{\mathbf{k}}-v_{\mathbf{k+q}}u_{\mathbf{k}}\right)^2}{E_{\mathbf{k}}+E_{\mathbf{k+q}}}. \tag{A-15}$$

Therefore, by using eqs. (A-14) and (A-15), we can obtain the aforementioned electromagnetic responses, which are infrared absorption, the paramagnetic

current, and the dielectric function. The importance of these two equations is that we have related them to the coherence factors $\left(u^2_{\mathbf{k+q}}v^2_{\mathbf{k}} - u_{\mathbf{k}}v_{\mathbf{k}}u_{\mathbf{k+q}}v_{\mathbf{k+q}}\right)$ and $\left(u_{\mathbf{k+q}}v_{\mathbf{k}} - v_{\mathbf{k+q}}u_{\mathbf{k}}\right)^2$, which in turn can be associated with the quantum metric as shown in chapter 4. This will allow us to associate each of these electromagnetic responses with the quantum metric and the fidelity number, providing us with the possibility of measuring them experimentally.

B
Electromagnetic responses for an non-interacting electron gas

In this appendix, we calculate some electromagnetic responses such as the electrical conductivity and the dielectric function for an electron gas with the aim of using the final equations obtained here for the case of singlet superconductors in chapter 4.

B.1
Electromagnetic perturbation

We will study how some quantities are modified when considering the electromagnetic field. First, we will begin with the current density operator

$$\mathbf{j}_\alpha = \frac{e}{\mathrm{V}} \sum_i \langle v_{i\alpha} \rangle, \tag{B-1}$$

where e is the electron charge, V is the volume, and $v_{i\alpha}$ represents the velocity of the i-th particle in the α direction. When considering the electromagnetic field, the velocity of the particles is modified in the following way

$$\mathbf{v}_i = \frac{1}{m} \left[\mathbf{p}_i - e\mathbf{A}(\mathbf{r}_i) \right]. \tag{B-2}$$

Then, the current considering the electromagnetic field has the following form [62]

$$\mathbf{j}_\alpha = \mathbf{j}_{\alpha 1} + \mathbf{j}_{\alpha 2}, \tag{B-3}$$

$$\mathbf{j}_{\alpha 1} = \frac{e}{m\mathrm{V}} \sum_i \langle p_{i\alpha} \rangle, \tag{B-4}$$

$$\mathbf{j}_{\alpha 2} = -\frac{e^2}{m\mathrm{V}} \sum_i A_\alpha, \tag{B-5}$$

where $\mathbf{j}_{\alpha 1}$ refers to the paramagnetic response of the material, hence it is called the paramagnetic current, this current is responsible for the decay of the current in the material; while $\mathbf{j}_{\alpha 2}$ refers to the diamagnetic response of the material [63].

In the case of the Hamiltonian, when we introduce a perturbation due to an electromagnetic field, the perturbative Hamiltonian has two components. The first is due to the scalar potential H_1' and the other part due to the vector

potential H_2', so it is expressed in the following way [44]

$$H' = H_1' + H_2', \tag{B-6}$$

$$H_1' = e \int d\mathbf{r}\, \rho(\mathbf{r})\phi, \tag{B-7}$$

$$H_2' = \int d\mathbf{r}\, j(\mathbf{r}) \cdot \mathbf{A}. \tag{B-8}$$

Depending on the electromagnetic response we want to calculate, we use linear response theory with the appropriate perturbative Hamiltonian considering the convenient gauge.

B.2 Electrical conductivity

We start from a system of electrons subject to an external electromagnetic field, this field induces a current, and the coefficient of linear response is the conductivity [44]

$$J_\alpha(\mathbf{r}, t) = \int dt' \int d\mathbf{r}' \sigma_{\alpha\beta}(\mathbf{r}, t; \mathbf{r}', t') E_\beta(\mathbf{r}', t'). \tag{B-9}$$

By performing a Fourier transform we can express eq. (B-9) as follows

$$J_\alpha(\mathbf{r}, t) = \sigma_{\alpha\beta}(\mathbf{q}, \omega) E_\beta(\mathbf{r}, t), \tag{B-10}$$

where $\sigma_{\alpha\beta}$ is the conductivity tensor that describes the current response in direction $\hat{\alpha}$ to an electric field applied in direction $\hat{\beta}$ and $E_\beta(\mathbf{r}, t) = |E_\beta| \exp i(\mathbf{q} \cdot \mathbf{r} - \omega t)$. The vector potential related to this electric field can be expressed as $A_\beta = (-i/\omega)|E_\beta| \exp i(\mathbf{q} \cdot \mathbf{r} - \omega t)$ considering a gauge where the electric potential is zero, because the final result does not depend on the gauge choice.

The Hamiltonian of this system has the following form $H = H_0 + H'$, where H_0 is the unperturbed system and H' is given by the eq. (B-8)

$$H' = \int d\mathbf{r} j_\alpha(\mathbf{r}, t) A_\alpha(\mathbf{r}, t), \tag{B-11}$$

where $\mathbf{A}_\alpha$ is the vector potential. As explained in appendix B.1, the form of the current changes when considering a vector potential, as indicated in eq. (B-3). Then, we now proceed to express this current by taking its expected value, as follows

$$\langle \mathbf{J}_\alpha \rangle = \langle j_\alpha(\mathbf{r}, t) \rangle + \frac{ie^2}{m\omega} E_\alpha(\mathbf{r}, t) \langle \rho \rangle_0, \tag{B-12}$$

where second term in the current is proportional to E_α linearly, and to calculate it, we must find the expected value of the density operator in the equilibrium state $\langle \rho \rangle_0$. On the other hand, to find $\langle j_\alpha(\mathbf{r}, t) \rangle$, we must use linear response theory, which leads to the following result

$$\langle j_\alpha(\mathbf{r},t)\rangle = \frac{-i}{\hbar}\int d\mathbf{r}\int_{-\infty}^{t} dt\langle[j_\alpha(\mathbf{r},t), H'(\mathbf{r}',t')]\rangle. \tag{B-13}$$

Replacing the perturbative Hamiltonian H' from eq. (B-11) into eq. (B-13), it can be verified by comparison with equation eq. (B-9) that the conductivity is left as [62, 44]

$$\sigma_{\alpha\beta}(\mathbf{r},t;\mathbf{r}',t') = \frac{i}{\omega}\left[\pi_{\alpha\beta} + \frac{e^2\langle\rho\rangle_0}{m}\delta(\mathbf{r}-\mathbf{r}')\delta_{\alpha\beta}\right], \tag{B-14}$$

where the term $\pi_{\alpha\beta}$ is called the current-current correlator and is defined as follows

$$\pi_{\alpha\beta} = \frac{i}{\hbar}\theta(t-t')\langle[j_\alpha(\mathbf{r},t), j_\beta(\mathbf{r}',t')]\rangle. \tag{B-15}$$

Then, we can observe that through linear response theory, we can obtain an expression for the electrical conductivity, which depends on the current-current correlator. The eq. (B-14) is important in our study since we are interested in calculating infrared absorption, which is an absorption process that represents the real part of the conductivity [44, 62, 63]. In turn, the real part of the conductivity is equivalent to taking the imaginary part of $\pi_{\alpha\beta}$ divided by the frequency

$$\mathrm{Re}\,\sigma_{\alpha\beta}(\mathbf{r},t) = \frac{1}{\omega}\mathrm{Im}\left[\pi_{\alpha\beta}(\mathbf{r},t)\right]. \tag{B-16}$$

Thus, this last equation will allow us to study infrared absorption. To be able to use it in s-wave superconductors, we would need to find the expression for $\pi_{\alpha\beta}$ for this type of superconductors, which will be carried out in chapter 4.

B.3 Dielectric response

In this section, we briefly present the most relevant equations related to the dielectric function that will be used in the dissertation. We will work in Gaussian units for calculating the dielectric response [56, 62].

Consider an electron gas into which an external electromagnetic disturbance is introduced. This causes the charges to reorganize and the system to become polarized. Due to this polarization, the field due to the disturbance is reduced, an effect known as screening [44, 62, 64]. The study of screening involves the dielectric function and the charge susceptibility, which we will show how their defining equations emerge below. Suppose we place an external potential V_{ext} in an electron gas, as a result, it induces a potential V_{ind}. Then, the total potential V_{tot} is the sum of both potentials

$$V_{tot}(\mathbf{r},t) = V_{ext}(\mathbf{r},t) + V_{ind}(\mathbf{r},t), \tag{B-17}$$

and the total charge density is given by

$$\rho_{e,tot}(\mathbf{r},t) = \rho_{e,ext}(\mathbf{r},t) + \rho_{e,ind}(\mathbf{r},t), \tag{B-18}$$

where we can relate each of the potentials to its charge density through the Poisson equation

$$-\nabla^2 V_{tot}(\mathbf{r},t) = 4\pi\rho_{e,tot}(\mathbf{r},t) \tag{B-19}$$

$$-\nabla^2 V_{ext}(\mathbf{r},t) = 4\pi\rho_{e,ext}(\mathbf{r},t) \tag{B-20}$$

$$-\nabla^2 V_{ind}(\mathbf{r},t) = 4\pi\rho_{e,ind}(\mathbf{r},t). \tag{B-21}$$

We will proceed to define the dielectric function $\varepsilon(\mathbf{q},\omega)$, after performing the corresponding Fourier transforms, as the linear response coefficient between the external potential and the total

$$V_{ext}(\mathbf{q},\omega) = \varepsilon(\mathbf{q},\omega)V_{tot}(\mathbf{q},\omega). \tag{B-22}$$

Now, we are going to define the charge susceptibility.

$$\rho_{e,ind}(\mathbf{q},\omega) = \chi(\mathbf{q},\omega)V(\mathbf{q},\omega). \tag{B-23}$$

Through the aforementioned equations, we can arrive at the following equation relating the dielectric function and the charge susceptibility

$$\epsilon(q) = 1 - \frac{4\pi}{q^2}\chi(\mathbf{k},\omega). \tag{B-24}$$

Next, we will calculate the charge susceptibility using linear response theory. First, we express the perturbative Hamiltonian, given by eq. (B-7), in second quantization after a Fourier transform as mentioned in [62] as

$$H' = \sum_{\sigma}\sum_{\mathbf{k},\mathbf{q}} V(\mathbf{q},t)c^{\dagger}_{\mathbf{k}+\mathbf{q}\sigma}c_{\mathbf{k}\sigma}, \tag{B-25}$$

where $V(\mathbf{q},\omega) = -e\phi(\mathbf{q},\omega)$, we will assume that this potential and the density operator oscillate coherently with the same frequency

$$V(\mathbf{q},t) = V(\mathbf{q},\omega)e^{-i\omega t}, \tag{B-26}$$

$$\langle\rho(\mathbf{q},t)\rangle = \langle\rho(\mathbf{q},\omega)\rangle e^{-i\omega t}, \tag{B-27}$$

where the density operator in momentum space is

$$\rho(\mathbf{q}) = \sum_{\sigma}\sum_{k} c^{\dagger}_{k+q\sigma}c_{k\sigma}. \tag{B-28}$$

We proceed to make use of linear response theory, where we arrive at the following relationship for the expected value of the density operator

$$\langle\rho(\mathbf{q},t)\rangle = -\frac{i}{\hbar}\int_{\infty}^{t} dt'\langle[\rho(\mathbf{q},t),H']\rangle. \tag{B-29}$$

We proceed to substitute H', eq. (B-25), into eq. (B-29). Subsequently, we apply the random phase approximation (RPA) and, taking into account the

definition of charge susceptibility given by eq. (B-23), we arrive at the following equation for the charge susceptibility, which in linear response theory is called the density-density correlator

$$\chi(\mathbf{k},\omega) = -\frac{i}{\hbar}\int_{\infty}^{t} dt' e^{i\omega(t-t')}\langle[\rho(\mathbf{q},t),\rho(-\mathbf{q},t')]\rangle. \tag{B-30}$$

The expression above, provides information about the dielectric response of the system when subjected to an electromagnetic perturbation.

C
Analytical expressions in s-wave superconductors

In this appendix, we will show the steps to obtain analytical expressions for quantum geometry and electromagnetic responses. To achieve this, we will consider a continuous model, assuming proximity to the Fermi surface, to express various terms, such as the dispersion energy $E_{\mathbf{k}}$ and the quantum metric $g_{\nu\nu}$ in their analytical forms. Subsequently, we will make some approximations to arrive at the analytical form of the fidelity number. For the case of electromagnetic responses, we will follow similar steps, which will be detailed in this appendix, focusing on the paramagnetic current response coefficient $K_1(\mathbf{q})$ and the term $P_0(\mathbf{q}, 0)$ of the dielectric function.

C.1
Analytical expressions for the quantum geometry

Quantum metric

We previously saw that the expression for the quantum metric for the case of s-wave superconductors is given by eq. (3-30). To derive an analytical expression, we will consider a continuous model assuming proximity to the Fermi surface. Thus, the dispersion energy can be expressed in the following way

$$E_k = \left[\left(\frac{k^2}{2m} - \frac{k_F^2}{2m} \right)^2 + \Delta^2 \right]^{1/2}, \tag{C-1}$$

using the coherence length $\xi = \hbar v_F/\pi\Delta = \hbar k_F/m\pi\Delta$ we can arrive at expressing it as follows

$$E_k \approx \Delta \left[1 + \frac{1}{2} \left(\frac{\pi\xi}{\hbar} \right)^2 (k - k_F)^2 \right]. \tag{C-2}$$

Now, we replace the eq. (C-2) in the quantum metric eq. (3-30), later we consider that $v_\mu = k\cos\theta/m$ and the following approximation for a small value of y

$$1/(1+y)^n \approx 1/(1+ny). \tag{C-3}$$

Obtaining the following expression

$$g_{\nu\nu} = \frac{\Delta^2 v_\mu^2}{4E^4} \approx \frac{(k\cos\theta/m)^2}{4\Delta^2\left[1+2\left(\frac{\pi\xi}{\hbar}\right)^2(k-k_F)^2\right]}. \tag{C-4}$$

In this way, we obtain the analytical expression of the quantum metric that will be used later on.

Fidelity number en 3D

In the case of the fidelity number, we will integrate the metric given by eq. (C-4) following the definition given in eq. (3-15) for 3D and 2D. First, we will start with the calculation in 3D

$$\mathcal{G}_{\mu\mu}^{3D} = \int \frac{d^3\mathbf{k}}{(2\pi)^3} g_{\mu\mu}. \tag{C-5}$$

Now, considering spherical coordinates $d^3\mathbf{k} = k^2\sin\theta\, dk\, d\theta\, d\varphi$ and solving the integrals for θ and φ we obtain

$$\mathcal{G}_{\mu\mu}^{3D} = \frac{1}{24\pi^2\Delta^2 m^2}\int_0^\infty dk\, \frac{k^4}{\left[1+\frac{1}{2}\left(\frac{\pi\xi}{\hbar}\right)^2(k-k_F)^2\right]^4}. \tag{C-6}$$

We proceed to make the change of variable $k = (2\pi\hbar/a)x$ and using the eq. (C-3), we can obtain the following expression

$$\mathcal{G}_{\mu\mu}^{3D} = \frac{1}{24\pi^2\Delta^2 m^2}\int_0^\infty dx\, \frac{\left(\frac{2\pi\hbar}{a}\right)^5 x^4}{1+8\pi^4\left(\frac{\xi}{a}\right)^2(x-x_F)^2}, \tag{C-7}$$

where we can express a part of the integrand with an extremely narrow Lorentzian, due to this we can approximate it to a delta function

$$\frac{1}{\left[1+2n\pi^4\left(\frac{\xi}{\hbar}\right)^2(k-k_F)^2\right]} = \frac{\eta^2}{\eta^2+(x-x_F)^2} \approx \pi\eta\delta(x-x_F), \tag{C-8}$$

where $\eta = a/\sqrt{2n}\pi^2\xi$. Using the approximation eq. (C-8) for $n=4$ in eq. (C-7) we have

$$\mathcal{G}_{\mu\mu}^{3D} = \frac{\sqrt{2}}{3}\frac{\pi^2\hbar^5}{\Delta^2 m^2 a^4\xi}\int_0^\infty dx\, x^4\delta(x-x_F), \tag{C-9}$$

$$\mathcal{G}_{\mu\mu}^{3D} = \frac{\sqrt{2}}{3}\frac{\pi^2\hbar^5}{\Delta^2 m^2 a^4\xi}\left(\frac{k_F}{2\pi\hbar/a}\right)^4, \tag{C-10}$$

where we apply the property of the delta function for the integral. Now we can reconfigure the last expression in such a way that it can be written as follows

$$\mathcal{G}_{\mu\mu}^{3D} = \frac{\pi^2}{6\sqrt{2}}\left(\frac{\xi}{a}\right)\left(\frac{k_F}{2\pi\hbar/a}\right)^2\left(\frac{\hbar}{a}\right), \tag{C-11}$$

this last equation shows us the analytical expression of $G^{3D}_{\mu\mu}$, and we can also verify that its units are correct.

Fidelity number in 2D

Now we will calculate the fidelity number for 2D following the definition given by eq. (3-15) for 2D

$$\mathcal{G}^{2D}_{\mu\mu} = \int \frac{d^2\mathbf{k}}{(2\pi)^2} g_{\mu\mu}. \tag{C-12}$$

we now consider polar coordinates $d^2\mathbf{k} = k \sin\theta \, dk \, d\theta$ and solving the integral for θ obtaining

$$\mathcal{G}^{2D}_{\mu\mu} = \frac{1}{16\pi\Delta^2 m^2} \int_0^\infty dk \, \frac{k^3}{\left[1 + \frac{1}{2}\left(\frac{\pi\xi}{\hbar}\right)^2 (k - k_F)^2\right]^4}. \tag{C-13}$$

We continue with a change of variable $k = (2\pi\hbar/a)x$ and considering the approximation given by eq. (C-3), we have

$$\mathcal{G}^{2D}_{\mu\mu} = \frac{1}{16\pi\Delta^2 m^2} \int_0^\infty dx \, \frac{\left(\frac{2\pi\hbar}{a}\right)^4 x^3}{1 + 8\pi^4 \left(\frac{\xi}{a}\right)^2 (x - x_F)^2}. \tag{C-14}$$

Again considering the approximation eq. (C-8) for $n = 4$ we have

$$\mathcal{G}^{2D}_{\mu\mu} = \frac{\sqrt{2}}{4} \frac{\pi^2\hbar^4}{\Delta^2 m^2 a^3 \xi} \int_0^\infty dx \, x^3 \delta(x - x_F) \tag{C-15}$$

$$\mathcal{G}^{2D}_{\mu\mu} = \frac{\sqrt{2}}{4} \frac{\pi^2\hbar^4}{\Delta^2 m^2 a^3 \xi} \left(\frac{k_F}{2\pi\hbar/a}\right)^3, \tag{C-16}$$

reconfiguring this last equation we can write it as follows

$$\mathcal{G}^{2D}_{\mu\mu} = \frac{\pi^2}{8\sqrt{2}} \left(\frac{\xi}{a}\right) \left(\frac{k_F}{2\pi\hbar/a}\right). \tag{C-17}$$

The expression above is the analytical expression of $G^{2D}_{\mu\mu}$ whose units are correct as it is just a dimensionless number, which is consistent with its definition.

C.2
Analytical expressions for the electromagnetic responses

Paramagnetic current

To calculate the analytical expression, they started with the definition for $K_1^{3D}(\mathbf{q})$, which is given by eq. (4-20)

$$K_1^{3D}(q) \approx -e^2q^2 \int \frac{d^3\mathbf{k}}{(2\pi\hbar)^3} v_\mu^2 \frac{g_{\nu\nu}}{E_\mathbf{k}}, \tag{C-18}$$

where $\hat{\nu}$ is the direction of $\mathbf{q} = q\hat{\nu}$ and $\hat{\mu}$ is the polarization direction. Now we will use spherical coordinates for the integral, we have the following expression

$$K_1^{3D}(\mathbf{q}) = -e^2q^2 \int_0^{2\pi} d\varphi \int_0^{\pi} d\theta \sin\theta \int_0^{\infty} \frac{dk}{(2\pi\hbar)^3} k^2 v_\mu^2 \frac{g_{\nu\nu}}{E_\mathbf{k}}. \tag{C-19}$$

Let's consider $\hat{\nu}$ in the angular integral, so we're going to use the following expression

$$v_\mu = \frac{k}{m}\cos(\theta - \alpha), \tag{C-20}$$

where α is the angle between the propagation direction $\hat{\boldsymbol{\mu}}$ and the polarization $\hat{\boldsymbol{\nu}}$. Next, we will replace eqs. (C-2), (C-4) and (C-20) in eq. (C-19), obtaining after solving the integral for φ and θ the following

$$K_1^{3D}(\mathbf{q}) = \frac{-2\pi e^2q^2 f(\alpha)}{(2\pi\hbar)^3 4m^4\Delta^3} \int_0^{\infty} dk \, \frac{k^6}{\left[1 + \frac{1}{2}\left(\frac{\pi\xi}{\hbar}\right)^2 (k - k_F)^2\right]^5}, \tag{C-21}$$

proceeding with a change of variable $k = (2\pi\hbar/a)x$ and considering the approximations given by eqs. (C-3) and (C-8), we obtain after solving the integral the following expression

$$\begin{aligned} K_1^{3D}(\mathbf{q}) &= -e^2 \frac{4\pi^6 f(\alpha)}{\sqrt{10}ma^3} \left(\frac{\xi}{a}\right)^2 \left(\frac{q}{2\pi\hbar/a}\right)^2 \left(\frac{k_F}{2\pi\hbar/a}\right)^3, \\ f(\alpha) &\equiv \frac{4}{15} + \frac{2}{15}\cos^2\alpha, \end{aligned} \tag{C-22}$$

where we can use the expression given by eq. (C-11) for the fidelity number in 3D, obtaining

$$K_1^{3D}(\mathbf{q}) = -\frac{288\pi^2}{\sqrt{10}} \frac{f(\alpha)e^2}{ma^3} \left(\frac{q}{2\pi\hbar/a}\right)^2 \left(\frac{k_F}{2\pi\hbar/a}\right)^{-1} \left(\frac{\mathcal{G}_{\nu\nu}^{3D}}{\hbar/a}\right)^2. \tag{C-23}$$

Thus, obtaining the analytical expression for $K_1^{3D}(\mathbf{q})$. For the 2D case, the approach is similarly executed, once again utilizing the expression provided by eq. (C-20) for v_μ and this time evaluating the integral in polar coordinates, yielding as a result

$$\begin{aligned} K_1^{2D}(\mathbf{q}) &= -\frac{2\pi^5 e^2 \overline{f}(\alpha)}{\sqrt{10}ma^2} \left(\frac{q}{2\pi\hbar/a}\right)^2 \left(\frac{\xi}{a}\right)^2 \left(\frac{k_F}{2\pi\hbar/a}\right)^2, \\ \overline{f}(\alpha) &\equiv \frac{\pi}{4} + \frac{\pi}{2}\cos^2\alpha, \end{aligned} \tag{C-24}$$

where using eq. (C-17), we can express it in terms of the fidelity number in 2D

$$K_1^{2D}(\mathbf{q}) = -\frac{2\pi^5 e^2 \overline{f}(\alpha)}{\sqrt{10}ma^2} \left(\frac{q}{2\pi\hbar/a}\right)^2 (\mathcal{G}_{\nu\nu}^{2D})^2. \tag{C-25}$$

Hence, we have obtained an analytical expression for $K_1^{2D}(\mathbf{q})$.

Linear screening

To obtain an analytical expression for P_0^{3D}, we start from eq. (4-25)

$$P_0^{3D}(\mathbf{q},0) \approx -q \int \frac{d^3\mathbf{k}}{(2\pi\hbar/a)^3} \frac{g_{\nu\nu}}{E_{\mathbf{k}}}. \tag{C-26}$$

Now, we consider spherical coordinates for the integral, obtaining

$$P_0^{3D}(\mathbf{q},0) = -q \int_0^{2\pi} d\varphi \int_0^{\pi} d\theta \sin\theta \int_0^{\infty} \frac{dk}{(2\pi\hbar/a)^3} k^2 \frac{g_{\nu\nu}}{E_{\mathbf{k}}}. \tag{C-27}$$

We proceed by substituting eqs. (C-2) and (C-4) into eq. (C-27), obtaining after solving the integral for φ and θ the following expression

$$P_0^{3D}(\mathbf{q},0) = -\frac{\pi q^2}{3(2\pi\hbar/a)^3\Delta^3 m^2} \int_0^{\infty} dk \frac{k^4}{\left[1 + \frac{1}{2}\left(\frac{\pi\xi}{\hbar}\right)^2 (k-k_F)^2\right]^5}. \tag{C-28}$$

Now, we perform the change of variable $k = \frac{2\pi\hbar}{a}x$ and apply the approximations given by eqs. (C-3) and (C-8), proceeding to solve the integral, which yields the following result

$$P_0^{3D}(\mathbf{q},0) = -\frac{4\pi^4}{3\sqrt{10}\Delta} \left(\frac{\xi}{a}\right) \left(\frac{k_F}{2\pi\hbar/a}\right)^2 \left(\frac{q}{2\pi\hbar/a}\right)^2. \tag{C-29}$$

We can relate the expression above to the fidelity number using the eq. (C-11), obtaining

$$P_0^{3D}(\mathbf{q},0) = -\frac{8\pi^2}{\sqrt{5}\Delta} \left(\frac{q}{2\pi\hbar/a}\right)^2 \frac{\mathcal{G}_{\nu\nu}^{3D}}{\hbar/a}. \tag{C-30}$$

In this manner, we obtain the analytical expression for $P_0^{3D}(\mathbf{q},0)$. For the 2D case, we proceed in the same manner, with the distinction that polar coordinates must be employed, yielding the following result.

$$\begin{aligned} P_0^{2D}(\mathbf{q},0) &= -\frac{\pi^4}{\sqrt{10}\Delta} \left(\frac{\xi}{a}\right) \left(\frac{k_F}{2\pi\hbar/a}\right) \left(\frac{q}{2\pi\hbar/a}\right)^2, \\ P_0^{2D}(\mathbf{q},0) &= -\frac{8\pi^2}{\sqrt{5}\Delta} \left(\frac{q}{2\pi\hbar/a}\right)^2 \mathcal{G}_{\nu\nu}^{2D}. \end{aligned} \tag{C-31}$$

For this last expression, we have utilized eq. (C-17) for the fidelity number, thereby presenting an analytical expression for $P_0^{2D}(\mathbf{q},0)$.